ALMA MATER STUDIORUM
UNIVERSITÀ DI BOLOGNA

DIPARTIMENTO DI INGEGNERIA INDUSTRIALE

CORSO DI LAUREA MAGISTRALE IN

INGEGNERIA ENERGETICA

MODELLING THE PLASMA CHEMISTRY OF HCN FORMATION BY CH_4/NH_3 PLASMA

Tesi di laurea magistrale *Applicazioni industriali dei plasmi (M)*

Relatore

Ch.mo Prof. Matteo Gherardi

Presentata da

Maristella Massaro

Correlatori

Prof. Annemie Bogaerts

Prof. Romolo Laurita

Dr. Eduardo Morais

Andrea Marchetti

Sessione invernale Marzo 2024

Anno Accademico 2022/2023

1 Introduction

1.1 Industrial HCN production

Hydrocyanic acid (HCN) is widely used in medicine, in metallurgy, and for pesticides, fuel, and polymer production. BASF Corporation established the first plant for the industrial production of HCN in the 1950s, driven by the demand for plastics and polymers such as nylon and Plexiglass (1). The annual HCN production in 1956 was only 2400 tonnes, but today it has increased to more than 100,000 tonnes per year (2). This increase in production is the result of the increasing demand and the development of complex processes involving HCN. The conventional industrial production of HCN, from NH_3 and CH_4, requires extremely high temperatures (> 1600 K). From an energetic, operational, and safety perspective, a drastic decrease in this process' temperature is highly desirable. In addition, in the future scenario of systems electrification (3) , it is imperative to study a new approach to produce HCN that can reduce CO_2 emissions and avail of green electricity. In this context, plasma emerges as a promising technology to assist in the production of HCN.

Another industrially relevant product from the CH_4 + NH_3 reaction is acetonitrile C_2NH_3, which is the simplest organic nitrile, and akin to HCN, contains the group C≡N. Acetonitrile is an aprotic polar solvent and it is also widely used in many industrial and pharmaceutical processes (4). Indeed, it is mainly used as a solvent in the purification of butadiene in refineries, but it is also used to synthesise pharmaceuticals, perfumes, rubber products, pesticides and batteries. Furthermore, it is used to extract fatty acids from animal and vegetable oils (5).

1.2 Plasma as a green alternative for gas conversion

Plasma is a very reactive environment, suitable for many applications such as the chemical conversion of gases. The non-equilibrium character of non-thermal plasmas enables some thermodynamically unfavourable chemical reactions at relatively low temperatures (3). The plasma-generated electrons, through collisions, can activate and dissociate reactant molecules (e.g., CH_4 and NH_3) which will in turn trigger chemical reactions of the produced radicals, leading to different products such as HCN, H_2 or C_2NH_3. For these reasons, the reactants may not require to be thermally activated at high temperatures, hence the process can be carried out at a few hundred Kelvins. At present, plasma-assisted gas conversion

processes must be further developed by optimizing the reaction conditions (e.g., power and flow rate, which determines residence time) and plasma characteristics (type of discharge, electron temperature, gas temperature, etc) in order to achieve better energy efficiency, conversion and selectivity and eventually be implemented in industry.

1.3 CH_4 and NH_3 plasma conversion – state of the art

To our knowledge, HCN production using plasma without catalyst has only been reported once in the literature. Thus, the current the state-of-the-art is based on a single study by Yi et al. (3) who proposed a series of experiments for HCN synthesis using plasma catalysis. The aim of the work was to test which catalyst showed best performance in terms of HCN yield and selectivity. The study demonstrated the feasibility of plasma-catalytic ammonia reforming of methane (ARM) at 673 K to produce HCN and H_2 using $CH_4 + NH_3$ plasmas in a dielectric barrier discharge DBD reactor (more details to follow) packed with copper-based catalysts. It also highlighted the potential for further optimizing the plasma-driven process to reduce the energy cost by adjusting reaction conditions, catalysts, and plasma properties such as reduced electric field and electron temperature. In addition, this work also presents a single case in which plasma alone was used in this process with a conversion of ~ 12% for methane. More specifically, Yi et al. have reported the formation of two main products HCN and C_2NH_3 (acetonitrile), with a selectivity ~ 60 % and ~20 %, respectively.

1.4 Gas-phase kinetic modelling of a DBD plasma

Plasma modelling involves describing the behaviour of a large number of individual particles, including electrons, ions, radicals, atoms and molecules, both in the ground state and in excited levels, as they move within the plasma under the influence of electromagnetic forces (6) (7). Modelling a plasma discharge is helpful to understand the behaviour and properties of non-thermal, quasi-thermal and thermal plasmas, leading to optimized plasma-driven processes and the birth of new technologies.

Indeed, it is useful to gain information, such as species densities and temperatures, and to study the interplay between key parameters. In turn, this is important for investigating the synthesis of the main products since their selectivity and the degree of conversion from the reagents involved can be deduced from the modelling results. Zero-dimensional plasma modelling is also useful to investigate the multitude of chemical pathways involved in a

plasma-assisted process. In other words, the simulations allow us to develop an understanding of reaction mechanisms, thus offering insights into beneficial and limiting chemical processes for products of interest, HCN in this thesis.

In this study, the plasma chemistry solver consists of a solver of ordinary differential equations (ODE) coupled with a solver for the Boltzmann equation for electrons. The ODE solver will integrate *n+1* equations, *n* of which are particle balances (one for each chemical species featured in the model) and the plus one refers to the energy balance of the gas phase. The Boltzmann solver allows the system to compute the electron energy distribution function (EEDF) which determines the reaction rates of the electron impact processes.

The DBD configuration possesses essential advantages in surface processing and plasma chemistry. DBD is a low-temperature discharge, usually operated at atmospheric pressure. DBD plasmas are typically obtained between two parallel electrodes separated by a gap of some millimeters and excited by alternating current (AC) voltage with frequency in the range of 1–500 kHz (8).

To optimize the yield of the HCN product and develop an understanding of the reaction mechanisms involved in HCN formation in the plasma-assisted CH_4 + NH_3 process, a zero-dimensional kinetic modelling approach will be utilised. This model will be evaluated with the ZDPlasKin plasma chemistry solver, and the modelled outputs will allow for the investigation of the most profitable operating conditions.

2 Zero-dimensional plasma modelling

In this section, the numerical methodology used to model the DBD plasma is presented, and the considered chemistry, solvers and modelling approaches are discussed.

2.1 General aspects of global modelling

Before explaining the model, it is necessary to outline the species present in a plasma environment:

- Electrons: negatively charged subatomic particles;
- Ions: atoms or molecules that have lost or gained one or more electrons, resulting in a net positive or negative electric charge;
- Neutral atoms and molecules: uncharged particles that are present in the plasma. These can be stable molecules (ground state and rotationally, vibrationally and electronically excited species) or radicals, which have an unpaired electron, and are therefore more reactive.

In plasma modelling, neutral species and ions are considered heavy particles and they play a significant role. Indeed, while the electrons typically initiate the chemistry, by electron impact ionization, excitation and dissociation, the heavy particles further contribute to the chemistry, by many chemical reactions (9). The elaboration of a reaction network is decisive for 0D modelling because it lays the foundation for analysing the system using a differential equation solver. This solver uses numerical methods to approximate the solutions of ODEs, providing valuable information on the behaviour and dynamics of the system (e.g. temporal evolution of the concentrations of neutral species and ions, the energy distribution of particles, and the rates of ionization and various chemical reactions). It can also help in analysing the stability of the plasma system and the impact of external factors, such as electric and magnetic fields, on the plasma behaviour.

In order to build a model to describe a plasma medium, it is necessary to make decisions about what to include, and what to neglect, considering all the limitations and assumptions which are inherent to all models. In particular, it is important to analyse the geometry of the plasma reactor, the method by which power is deposited in the plasma system, if the plasma is

powered through DC or AC (in the second case, the frequency must be known). In addition, we must consider the gas or the gas mixture used to create the plasma (with its respective properties), the electron energy distribution function, as well as all species created in the plasma region, such as neutral particles and ionic species.

Solutions to equations in a global model must be found through numerical methods performing a direct numerical integration of equations over a given period.

The primary aim of global modelling is often to understand systems composed of a complex chemistry. For that reason, incorrect rate coefficients and cross sections can lead a significant negative impact on the accuracy of the outputs from the simulations. The method chosen to simulate the plasma conditions is a zero-dimensional method, based on balance equations that do not take into account spatial derivatives, so as to obtain maximum computational efficiency. The model outcomes and insights, along with the computational efficiency of this method, are amongst the reasons to continue to exploit the potential of this method for plasma systems.

2.2 Construction of a global model

One of the most substantial parts of the global model is the construction of the set of chemical reactions to be analysed. In fact, it is very important to consider all the chemical species involved in the overall process under investigation (CH_4 + NH_3) and to analyse all the possible reactions that could occur in the particular modelled conditions. In other words, the molecules of the feed gas (CH_4 and NH_3) can dissociate in the plasma and generate many different CH_x and NH_x radicals and ions, which in turn can recombine, leading to a variety of carbon- and nitrogen-coupled products. So, it is clear that many different molecule combinations will follow, and we must consider all of them. Once all the species involved and all possible reactions have been added, it is crucial to ensure that accurate reaction rate coefficients are available for the conditions being investigated. There are multiple sources for rate coefficients and cross sections in the literature, so at times it can be challenging to select the most suitable alternative. On the other hand, the rate coefficient of some reactions (especially those of radical-radical recombination) may not be available due to the scarcity of experimental data, which is oftentimes related to challenges in carrying out these experiments.

Reaction rate coefficients can be a function of gas temperature and pressure in the case of heavy particles (neutral-neutral recombinations but also for many reactions involving ionic species), and electron temperature in the case of electron collision processes. Again, rate coefficients may not be readily available (particulary for reactions involving ions and excited states), so in that case we must make estimations through careful approximations.

Excited states also play an important role in influencing the plasma dynamics. There are three different types of excitation: electronic, rotational and vibrational. All of those can be significant in both high and low pressure conditions but, a particularly decisive role is played by vibrational excitation, which represents an important channel for the loss of electron energy, as well as an important intermediate step in some reactions (10). Vibrational excitation is also important because the excited molecules usually have a higher dissociative attachment cross section (compared to ground state molecules), meaning that their presence can enhance the production of negative ions, such as H^- ions, in plasmas containing H_2 (11) (12). Akin to rate coefficients, experimental data is often unavailable for cross sections, so it is necessary to estimate or calculate them from approximations or from already measured cross sections.

2.2.1 Characteristics of a DBD zero-dimensional model

To date, the plasma technology most widely used to investigate both ammonia synthesis and also its breakdown, is the atmospheric pressure dielectric barrier discharges (DBD). This is commonly used in industry for efficient and small-scale processes (13). This technology has already been studied extensively with the zero-dimensional modelling approach, both with plasma alone and with the presence of a catalyst in the gap between the electrodes (14) (15) (16). As previously mentioned, in this type of modelling, it is assumed that the plasma is homogeneous and all spatial derivatives are zero. However, in reality DBD plasma systems can exhibit non-uniform micro-discharges and spatial gradients, which are not straightforward to be described by global models.

Modelling micro-discharges is also a challenging task due to the arbitrary nature of some of the parameters involved, such as the number of micro-discharge filaments (or pulses), the pulse duration and the pulse period. While these parameters are crucial in the model, their experimental determination can be difficult and imprecise, sometimes leading to inaccuracies in the modelled results. To address this issue, in this work, we modelled micro-discharges as

triangular power density pulses with a certain duration. Hence, we have both temporally and spatially distributed filaments, which only occupy a small portion of the total discharge volume. Because of the spatial and temporal behaviour of micro-discharges, not all pulses occurring in the plasma reactor (during a given residence time) affect the gas molecules passing through the reactor. In other words, it is impossible for a single molecule to be exposed to all the micro-discharges occurring in the reactor during their residence time. This means that the plasma power deposited into the reactor (through the micro-discharges) is not uniformly experienced by every single molecule in the reactor. For this reason, in the model, the power distribution factor (γ) is introduced to assign only part of the plasma power to micro-discharges (10). This is used to set the minimum power density based on the maximum power density:

$$p_{min} = \gamma \cdot p_{max} \tag{1}$$

with γ = 1 yielding a fully uniform plasma (composed of a weak continuous glow along the entire reactor), while γ = $1x10^{-6}$ yields a very filamentary plasma. The plasma kinetic model assumes that the micro-discharges are uniformly distributed in time in the plasma reactor.

2.2.2 Governing equations and computational tools

There are several codes available to solve global models for different sets of plasma conditions. In my case, the 0D plasma kinetics solver ZDPlaskin (17) was adopted to perform the simulations and achieve the aim of the thesis project.

The plasma kinetics solver evaluates the continuity equation (2) for the various species *p* with number density $n_p(\mathrm{t})$ (as a function of time) in a system with a user defined reaction scheme (18):

$$\frac{dn_p}{dt} = \sum_r c_{r,p} k_r \prod_q n_q \tag{2}$$

Where $c_{r,p}$ is the stoichiometry number of species *p* in reaction *r*, k_r is the rate coefficient and *q* are the colliding species in reaction *r*. The rate coefficients, k_r, are taken from literature,

often as a function of the gas or electron temperature (this was highly facilitated by PLASMANT's expertise in this field), or they are evaluated from electron impact cross sections and the electron energy distribution function (EEDF) through BOLSIG+, a numerical solver of the steady-state Boltzmann equation for electrons. The latter operates in tandem with ZDPlaskin, since it requires the collision cross sections (oftentimes procured from the open-access database LXCat) (19), the reduced electric field (E/N) (input given by ZDPlasKin to derive the EEDF), and the gas temperature as inputs. Subsequently, the mean electron energy is extracted from the EEDF to calculate the rate coefficients for electron impact reactions. The electric field E required by BOLSIG+ to solve the Boltzmann equation is calculated via the differential of the Joule heating equation (20):

$$\frac{dP}{dV} = J \cdot E = \sigma \cdot E^2 \tag{3}$$

Where P is the power deposited in a volume element V; $J = \sigma\ E$ is the current density with σ as the electron conductivity calculated by $\sigma = e \cdot n_e \cdot \mu_e$ (e is the elementary charge, n_e is the electron density, μ_e is the electron mobility calculated by BOLSIG+). Finally, the reduced electric field is calculated using the following expression (20):

$$\left(\frac{E}{N}\right) = \frac{1}{N}\sqrt{\frac{P}{\sigma}} \tag{4}$$

in which N is the total number density of species in the gas phase (N = 1.09 x 10^{19} cm^{-3} at 1 bar and 673 K).

2.2.3 Key parameters

As previously discussed, the kinetic modelling of a DBD plasma requires preliminary information, such as the power density as a function of time, from which the value of the generated electric field can be derived; the number of micro-discharges; the duration of power pulses (which represent the micro-discharges, when converting the spatial behaviour in the DBD into temporal behaviour for the global model, the temperature profile; the reactor characteristics and the power density distribution factor.

Typically, in DBD models, the temperature of the gas phase is assumed to be fixed and equal to that measured in the experiments (3). Although this is not entirely realistic, it is a fair

approximation for the model since experimental determination of local temperature profiles in DBD plasmas is not yet feasible. However, it is important to always bear in mind that this may lead to subsequent inaccuracies in the model. As DBD plasmas are non-thermal, the investigated gas temperatures should lie in the range of 400-700 K.

Another important parameter to consider is the residence time, which is the time that a reactant spends in a plasma reactor. Longer residence times can lead to higher conversion, but there is a limit beyond which the conversion does not increase further, because the system reaches steady state (forward and backward reaction rates become equal). The influence of residence time on conversion depends on various factors such as the type of plasma, the type of reactants, and the operating conditions of the plasma reactor (21).

2.3 Assumptions and limitations of the model

Modelling accurate chemical kinetics in plasma discharges, especially when they exhibit filamentary character, poses significant challenges. To simulate DBD filamentary discharges in a 0D framework, assumptions about the plasma volume, a constant gas temperature, and the number of micro-discharge pulses experienced by the gas molecules during their residence time in the reactor had to be made. In my specific case, we chose to fix the gas temperature at 673 K, since this is the measured reactor temperature in the CH_4/NH_3 DBD plasma described in the work of Yi et al. (3).

Also, there are some specific limitations which are inherent to the development of global models. For example, we do not consider conduction, convection and diffusion phenomena and this certainly limits the accuracy of the results. Regarding the EEDF, it cannot be obtained self-consistently in global models and this has a significant effect on the solutions. To have a realistic representation of this parameter, BOLSIG+ (21) considers electrons to be in equilibrium with the local reduced electric field. The validity of this assumption depends on the pressure linked to the electron impact cross sections for the gas being modelled. Furthermore, as we have already pointed out, the model assumes to consider a specific number of micro-discharges, as an approximation to the number of micro-discharge pulses that gas molecules can experience in the reactor. Finally, assuming a fixed gas temperature throughout the simulations may not accurately predict the behaviour of the chemical kinetics, since in reality local) increases in the gas temperature are expected.

Despite the approximations and inherent limitations, global modelling is an easy and effective approach to describe plasma dynamics, especially from a chemical kinetic perspective.

2.4 Model validation

As previously mentioned, the only experimental work which is available for direct validation of our model was carried out by Yi et al. (3). The methane conversion and the selectivity of the two main products reported in their work can be found in Figure 1.

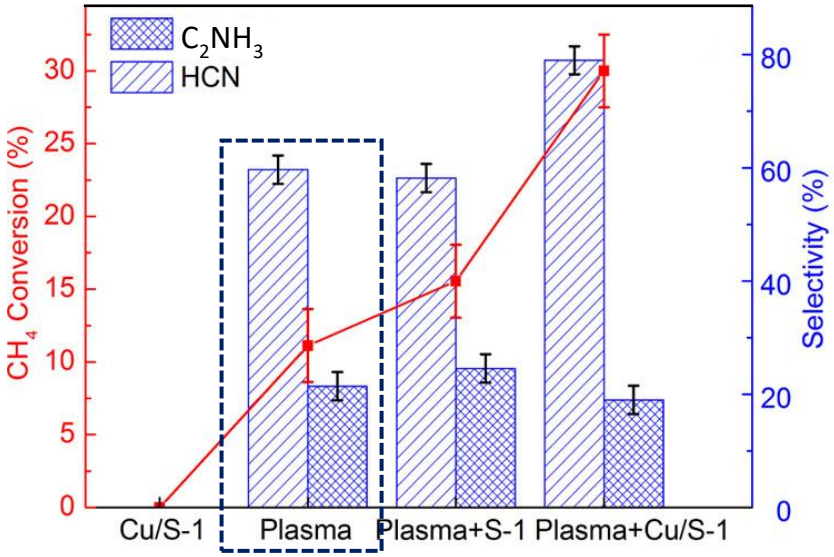

Figure 1. The CH_4 conversion and HCN and C_2NH_3 selectivity reported by Yi et al. (5), at 673K. The figure has been adapted to highlight (in the dashed box) the experimental case (only plasma) to which we refer for model validation

As indicated in the plot (for the plasma alone condition), in the absence of a catalyst, the experimentally measured CH_4 conversion was ~ 12% and, and the HCN and C_2NH_3 selectivity was ~60% and ~20%, respectively.

For validation of the model in terms of NH_3 conversion, we refer to the study conducted by Bang et al. (22) (Figure 2). In their work, several models were constructed and analysed to study the plasma-assisted cracking of NH_3 and to compare with available experimental data. Figure 2 shows their results for NH_3 conversion as a function of the gas temperature.

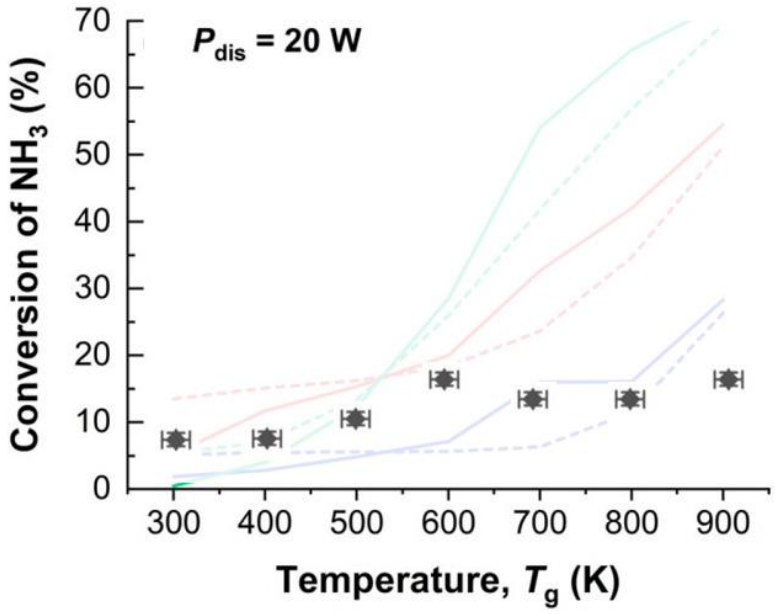

Figure 2. Experimental NH_3 conversion as a function of the gas temperature. The input power is 20 W, which is slightly different from the model at 17 W. This figure is an adaptation of the plots shown in Bang et al. (22). Colored solid line are model results with E/N experimental values, instead of dashed ones which are model result with a fixed E/N = 150 Td. The blue lines represent the kinetic model for NH_3 combustion using Zhang et al. chemistry set. The red lines represent the kinetic model for NH_3 pyrolysis using Alturaifi et al. chemistry set. The green lines represent the kinetic model for NH_3 synthesis using Van't Veer et al. chemistry set.

Looking at the temperature range of 600-700 K, a value for NH_3 conversion in the range of 10-20% is anticipated for the validation of our model.

3 Thesis objective

The objective of this thesis is to model the chemical kinetics in zero dimensions of the plasma-chemical process of HCN production from methane and ammonia streams, with subsequent validation of the model through comparison with published experimental results from similar systems.

The thesis activity initially focused on the construction of the chemical model, starting from two reaction sets already present in the PLASMANT research group's database. In fact, two already validated sets were used. The first was a set of reactions comprising methane and hydrogen-related species, and the second comprising ammonia and hydrogen-related species. The first step was to combine these sets and simultaneously reduce the number of species involved, in order to achieve a test case with sufficient computational efficiency to trial the model. The second step was to expand the existing sets by including reactions involving carbon, nitrogen and hydrogen ions and radical species, e.g. CNH_2, CNH_3, CNH_4, CNH_5, CN_2H, CN_2H_2, CN_2H_3, CN_2H_4, C_2NH_2, C_3NH_3, C_2NH_4, C_2NH_5, C_2NH_6. An important task carried out simultaneously was an improvement of the two already existing sets with updates on the rate coefficients from the most recent relevant literature (3) (22).

In the second part of this work, the model was constructed and the process was simulated with the abovementioned chemistry (the full list of species can be found in Table 1 and the list of reactions can be found in the Appendix). The outputs obtained were then analysed and compared with the few experimental datasets available in the literature. The collection of results has offered an insight into the species densities, mechanisms and pathways involved in HCN synthesis, allowing for reduction of the kinetic scheme and thus simplification of the model. For example, the analysis showed that the ions do not make a great contribution to the production of HCN, and those of minor interest were therefore removed from the chemical set.

As will be seen in the section 5, where we will discuss the results obtained, the model proposed in this thesis achieves good consistency with the current experimental data in the literature, allowing for the development of a better understanding of the complex chemistry of this process.

4 Methodology

4.1 ZDPlasKin and BOLSIG+ solver

ZDPlasKin is a package in Fortran 90, developed to solve zero-dimensional plasma chemistry kinetics. It has been developed by researchers at LAPLACE (Laboratoire des Plasmas et Conversion d'Energie) in the University of Toulouse (17). The software uses the DVODE solver from the ODEPACK collection of Fortran solvers for initial value problem ODE systems to compute particle densities and gas temperature (when calculated self-consistently). The solution of the Boltzmann equation for electron energy is achieved through the BOLSIG+ (23) software, also developed by researchers at LAPLACE. The coupling between these solvers enables conformity between the solutions of electron kinetics and chemical kinetics.

The software is structured in two main steps to minimise computational work, as summarised in Figure 3, where the components are depicted.

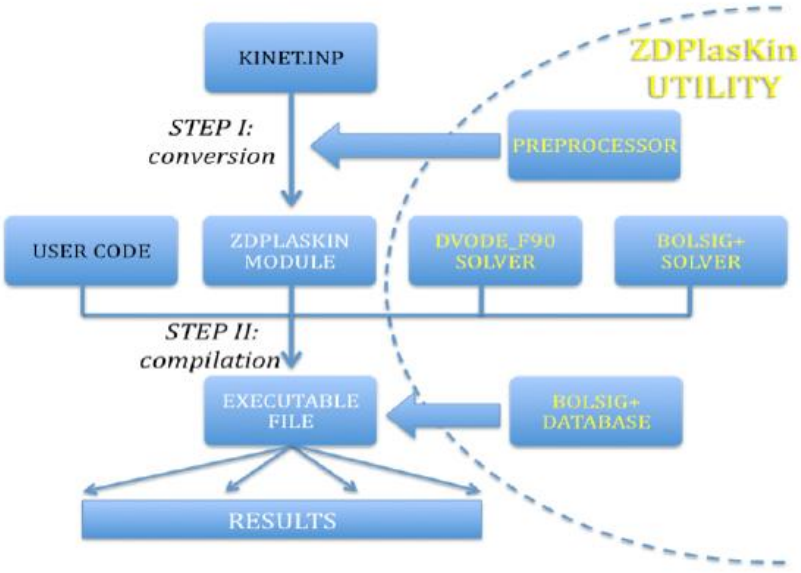

Figure 3. Summary diagram of the operation of ZDPlasKin (24)

In the first step, the *preprocessor* utility tool converts the file containing all the reactions (and reaction rate coefficients) under consideration (kinet.inp) into a Fortran module (zdplaskin_m.F90). In the second step, the user-built master code is employed, executing ZDPlasKin subroutines to perform time integrations and update reaction coefficients using BOLSIG+. This code is important because it provides the software with all the required information (such as power density and gas temperature) to solve the differential equations

characterising each reaction. In particular, two solvers are used: the first one, the DVODE, is used with the differential equations for each reaction. This solver evaluates the reactions over time considering the density of the species involved. It is an iterative process, hence at each new step it will use the solution (densities) obtained in the previous one.

The second solver, BOLSIG+, operates in the same fashion but for electron impact reactions, which do not have a rate expression but are characterised by a cross section, i.e. the probability of that event to occur. BOLSIG+ utilises the reduced electric field (calculated by ZDPlasKin using the power density given by the input power provided in the user code) and calculates the electron energy distribution function (EEDF) from which it derives the electron energy. This is necessary because the probability of electron collisions occurring, i.e. the cross section, is directly related to the energy of the electrons. Finally, BOLSIG+ passes the result to ZDPlasKin which, from the electron energy, evaluates the electron density, one of the main outputs of the software.

In addition to this, the software also provides time dependencies of key parameters such as reduced electric field, gas and electron temperature, reaction rates. Altogether, this contributes to building an understanding of the plasma dynamics and gain insights into HCN (and C_2NH_3) synthesis mechanisms from CH_4 and NH_3 feed streams.

4.2 Chemistry included in the model

In this study, the input gas is a mixture consisting of ammonia NH_3 and methane CH_4. It is necessary to investigate how CH_4 and NH_3 molecules interact with high-energy electrons, resulting in ionisation, dissociation, elastic collisions, attachment, electronic excitation and vibrational excitation reactions. These reactions produce the ions, radicals and excited C_xH_y and N_xH_y species shown in Table 1.

Table 1. Species considered in the model.

Stable molecules	Radicals	Ions and electrons	Excited species
CH_4 C_2H_2 C_2H_4 C_2H_6 C_3H_6 C_3H_8	C C_2 C_3 CH CH_2 CH_3 C_2H C_2H_3 C_2H_5 C_3H_5 C_3H_7	C^+ C_2^+ CH_3^+ CH_4^+ CH_5^+	
NH_3 N_2H_4	N NH NH_2 N_2H_3	N^+ NH^+ NH_2^+ NH_3^+ NH_4^+	$N(_2D)$ $N(_2P)$
H_2	H	H^+ H_2^+ H_3^+	
C_2N_2	CN CN_2 C_2N C_3N		
HCN CNH_3 CNH_5 CN_2H_2 CN_2H_4 C_2NH_3 C_2NH_5 C_2NH_7	CNH_2 CNH_4 CN_2H CN_2H_3 C_2NH_2 C_2NH_4 C_2NH_6	HCN^+ electrons	

Most of the electron impact cross sections for C_xH_y species were retrieved from PLASMANT's datasets. The cross sections for the reactions shown in Table 2, have been updated following the publication of new data by IST Lisbon (25).

Table 2. Reactions for which updated cross sections were used, following new data publication by IST Lisbon (25).

ELASTIC	$CH_4 + e^- \rightarrow CH_4 + e^-$
IONIZATION	$CH_4 + e^- \rightarrow CH_4^+ + e^-$
IONIZATION	$CH_4 + e^- \rightarrow CH^+ + 3H + e^-$
IONIZATION	$CH_4 + e^- \rightarrow H_2^+ + CH_2 + e^-$
IONIZATION	$CH_4 + e^- \rightarrow H^+ + CH_3 + e^-$
IONIZATION	$CH_4 + e^- \rightarrow C^+ + 4H + e^-$
IONIZATION	$CH_4 + e^- \rightarrow CH_3^+ + H + e^-$
IONIZATION	$CH_4 + e^- \rightarrow CH_2^+ + H_2 + e^-$
DISSOCIATION	$CH_4 + e^- \rightarrow CH + H_2 + H + e^-$

DISSOCIATION	$CH_4 + e^- \rightarrow C + H_2 + H_2 + e^-$
DISSOCIATION	$CH_4 + e^- \rightarrow CH_3 + H + e^-$
DISSOCIATION	$CH_4 + e^- \rightarrow CH_2 + H_2 + e^-$
DISSOCIATION	$CH_4 + e^- \rightarrow C + 2H_2 + e^-$
ATTACHMENT	$CH_4 + e^- \rightarrow CH_3 + H^- + e^-$
ATTACHMENT	$CH_4 + e^- \rightarrow CH_2^- + 2H + e^-$

For N_xH_y species, the cross sections for electron impact reactions reported in the work of Van 't Veer et al. (21) (i.e. those from the Hayashi database (26) on LXcat) were used.

Regarding the reaction set used for N_xH_y species interactions, some modifications were made in light of updates in the literature. Indeed, Bang et al. (22) noted that there should be several additional electron impact excitation processes that can lead to NH_3 dissociation, which were not be included in Hayashi's data set. As suggested by Bang et al., for dissociation of NH_3, instead of the rate expressions formerly used, we employed the NH_3 excitation cross sections leading to the excited state of maximum energy. Additionally, new pressure-dependent rate coefficients for 3-body recombination reactions were considered from Baulch et al. (27). In (22) the two NH_3 dissociation reactions - whose cross sections were assumed to be the same as the excitation to the NH_3 excited state of maximum energy – are listed.

Table 3. NH_3 reactions for which updated dissociation cross section are assumed in the model, equal to electron impact excitation of an excited state with maximum energy.

$e^- + NH_3 \rightarrow e^- + NH_2 + H$	(26)
$e^- + NH_3 \rightarrow e^- + NH + H_2$	(26)

The chemical reactions of CH_x and NH_x radicals will lead to the formation of C_2H_y, N_2H_y, and $C_xN_zH_y$ species. However, while the chemistries involving C-H and N-H species have been widely understood and validated (with rate coefficients available for nearly all reactions), the chemistry involving $C_xN_zH_y$ species is not well documented in the literature.

This quickly became a problem in this project. Our initial attempt to construct a set of reactions with the data available in online databases such as NIST (28) (for reactions between radical species) and UMIST (29) (for ion interactions) did not yield HCN and C_2NH_3 selectivity results consistent with the experiments. Therefore, when rate coefficients for reactions involving $C_xN_zH_y$ species were not available, assumptions have been made. In particular, for some $C_xN_zH_y$ species, as indicated in Table 4, we assumed a similar reactivity of the equivalent species with oxygen ($C_xO_yH_s$). In our opinion, this assumption is tenable because it is based on the fact that the reactivity of N_xH_y is similar to that of O_xH_y so the interactions, and the relative rate coefficients, with C_xH_y species are reasonably similar. Clearly, it was necessary to consider $C_xN_zH_y$ species and radicals that were homologous to $C_xO_yH_s$ species and radicals, i.e. with similar molecular structure.

In addition, the chemistry of O_xH_y is much better understood than that of N_xH_y, and this allowed us to extend the reaction scheme with a series of assumptions (reported in the Appendix) that allowed us to obtain more consistent results with the experimental ones.

Table 4. Original molecules with the O atom on the left and the analogous N-containing molecule on the right.

Original molecule	N-homologous molecule
O_2H 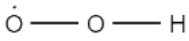	N_2H_3 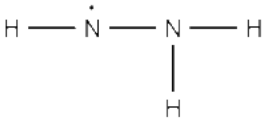
O_2H_2 	N_2H_4 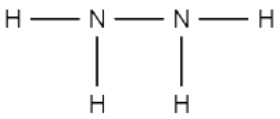
HCO 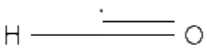	CNH_2 
CO_2H	CN_2H_3

	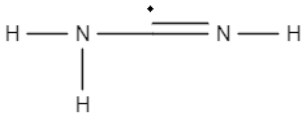
CO_2H_2 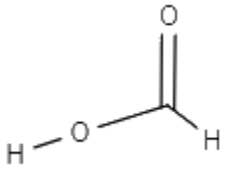	CN_2H_4 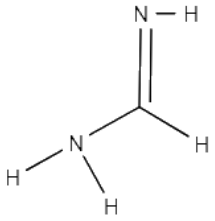
C_2OH_2 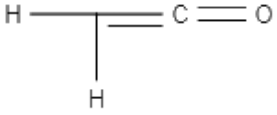	C_2NH_3 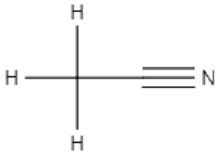
C_2OH_3 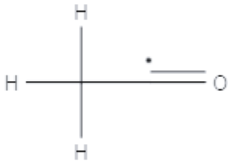	C_2NH_4 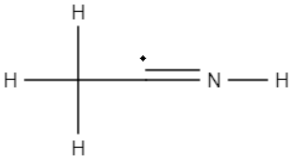
C_2OH_4 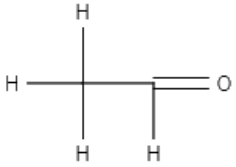	C_2NH_5 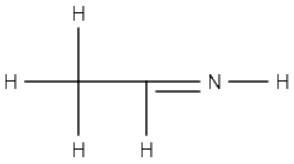
C_2OH_5 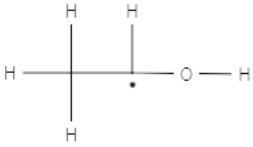	C_2NH_6 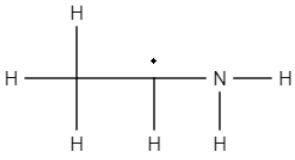

The reactions involving these species, alongside all other reactions considered in the chemical scheme of this model, are given in the Appendix.

4.3 Conversion and selectivity calculations

Conversion and selectivity are important metrics to be studied in order to verify how consistent the model is with the available experimental data. The conversion must be evaluated for each of the gases making up the input mixture, so in our case for both CH_4 and NH_3. In the present model, it is calculated as follows:

$$\mathrm{X_r} = \frac{C_{i,r} - \alpha \cdot C_{o,r}}{C_{i,r}} \times 100\% \tag{5}$$

Where $C_{i,r}$ and $C_{o,r}$ are the initial and final (outlet) concentration of the reactant under consideration, respectively, and α is the gas expansion factor, which is discussed below.

In general, most plasma reactors operate as plug-flow reactors, where the number of particles, concentrations and volumetric flow rates can alter along the reactor due to reactions. For example, in the reaction:

$$NH_3 + CH_4 \rightarrow HCN + 3\,H_2$$

the reactants NH_3 and CH_4 are converted into HCN and 3 H_2, thus with two molecules being transformed into four. This causes the volumetric flow rate to increase (as the pressure in the system is kept constant). Therefore, conversion and selectivity must be calculated based on the number of species entering and exiting the reactor per unit of time. The flux ratio or expansion factor α is used to determine the gas expansion ratio. For the implementation of α, we assume that the volumetric flow rates at inlet and outlet are obtained at the same temperature and pressure. Hence, α is also equal to the ratio of the total volumetric flow rates at outlet and inlet. In its simplest form α is given by the following equation (30):

$$\alpha = \frac{\dot{n}_{tot}^{out}}{\dot{n}_{tot}^{in}} = \frac{\dot{V}_{tot}^{out}}{\dot{V}_{tot}^{in}} \quad (6)$$

Where $\dot{n}_{tot}^{in}$ and $\dot{n}_{tot}^{out}$ are the total molar flow rate at the in- and outlet, respectively, and $\dot{V}_{tot}^{in}$ and $\dot{V}_{tot}^{out}$ are the volumetric flow rates at the in- and outlet, respectively. If α is neglected, the performance metrics will be seriously over- or underestimated.

Another important parameter to be evaluated is the selectivity of the reaction. In chemistry, the term selectivity (S_p) is defined as the ratio between the final density of the desired product and the amount of reagent consumed. It is calculated as follows for each product (20):

$$S_p = \frac{\beta \cdot \alpha \cdot C_{o,p}}{C_{i,\mathrm{r}} - \alpha \cdot C_{o,\mathrm{r}}} \times 100\% \quad (7)$$

Where β is the ratio of the number of atoms contained in the product of the element under consideration to the number of atoms of the same element in the reactant. If there are more than one reactant, β must be calculated for each one. $C_{i,r}$ and $C_{o,r}$ are the initial and final (outlet) concentration of the reactant. $C_{o,p}$ is the final (outlet) concentration of the product for which selectivity is calculated. α is the expansion factor defined above.

In order to make the definition of selectivity clearer, the equations used to calculate the nitrogen selectivity for the two main products in this study is provided below.

$$S_{C_2NH_3} = \frac{1 \cdot \alpha \cdot C_{o,C_2NH_3}}{C_{i,NH_3} - \alpha \cdot C_{o,NH_3}} \times 100\% \quad (8)$$

$$S_{HCN} = \frac{1 \cdot \alpha \cdot C_{o,HCN}}{C_{i,NH_3} - \alpha \cdot C_{o,NH_3}} \times 100\% \quad (9)$$

It is clear that in my case, regarding nitrogen selectivity, β is equal to 1 for both HCN and C_2NH_3.

5 Results and discussion

5.1 Modelled plasma characteristics

To match the experimental conditions, the ratio of the two gases in the input mixture was kept constant in all simulations performed: 33.3% of CH_4 and 66.7% of NH_3, and the gas flow rate was also fixed at 60 mL/min or 10^{-6} m^3/s (3). From the geometry of the reactor used by Yi et al. in the conversion experiments (shown in Figure 4), it was possible to calculate the reactor volume (see below), and in turn the residence time, which was approximately 4 s in all experiments.

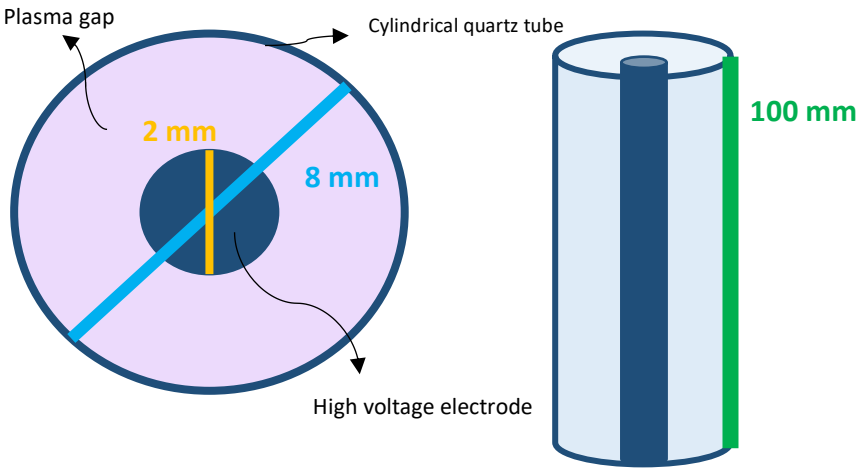

Figure 4. DBD experimental reactor. Transversal view of the quartz cylinder tube on the left. On the right the longitudinal view. (3)

20 ml/min -> CH_4 volumetric flowrate

40 ml/min -> NH_3 volumetric flowrate

Reactor volume (V_R) = 3992.38 mm^3 = 3.9924 x10^{-6} m^3

Total volumetric flowrate (Q_V) = 60 ml/min = 10^{-6} m^3/s

Residence time = $\frac{V_R}{Q_V}$ ≈ **4 s**

In addition, the following parameters were kept constant in our DBD model: the modelled number of micro-discharges is 100, the gas temperature is 673 K, pressure is 1 bar and the input power is 17 W.

While the input power, gas temperature and pressure are directly extracted from the available experimental data, the number of micro-discharges cannot be experimentally assessed. However, the choice to run the simulations with 100 micro-discharges is not arbitrary. In fact, the model was analysed for a range of numbers of micro-discharges to identify the value which yielded the best results in terms of CH_4 conversion (compared to the experiments). Figure 5 shows the CH_4 conversion and HCN selectivity results obtained from simulations carried out with varying numbers of micro-discharges, ranging between 30 and 150.

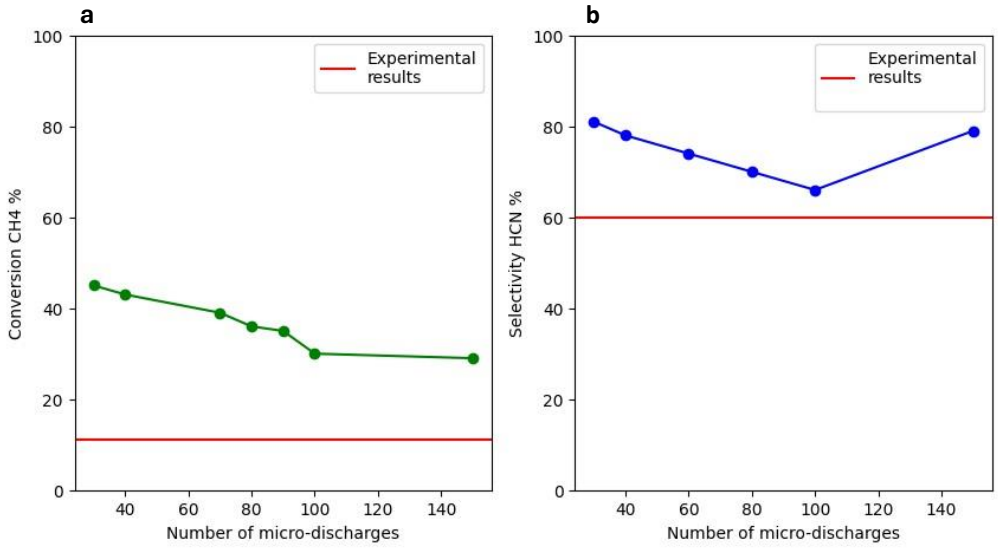

Figure 5. (a) CH_4 conversion model results (in green) against experimental ones (in red) over different numbers of micro-discharges. (b) HCN selectivity model results (in blue) against experimental ones (in red) over different numbers of micro-discharges.

The experimental results of Yi et al. (3) showed a methane conversion (for conditions similar to those studied with this model) of ca. 11.1%. From Figure 5.a, we can see that for a number of micro-discharges greater than 100, no significant improvement was observed. By setting this value at 100, the model predicts CH_4 conversion values that agree the most with those from the experiments. The number of micro-discharges not only influences CH_4 conversion, but also affects HCN selectivity. Figure 5.b shows a comparison between modelled results (in blue) and experimental results (in red). As can be seen, increasing the number of micro-discharges beyond 100 compromises agreement with the experimental results. Therefore, the value chosen represents a compromise to achieve fairly consistent values for both CH_4 conversion and HCN selectivity.

The time-resolved power density profile, constructed and implemented in the model to emulate the pulsed plasma micro-discharges in DBD reactors, is shown in Figure 6, both in the

first 0.5 s of the residence time (on the left) and for a shortened timescale to evidence the pulse shape (on the right). Figure 6.b shows the characteristic symmetrical triangle shape of the pulse type modelled in this study.

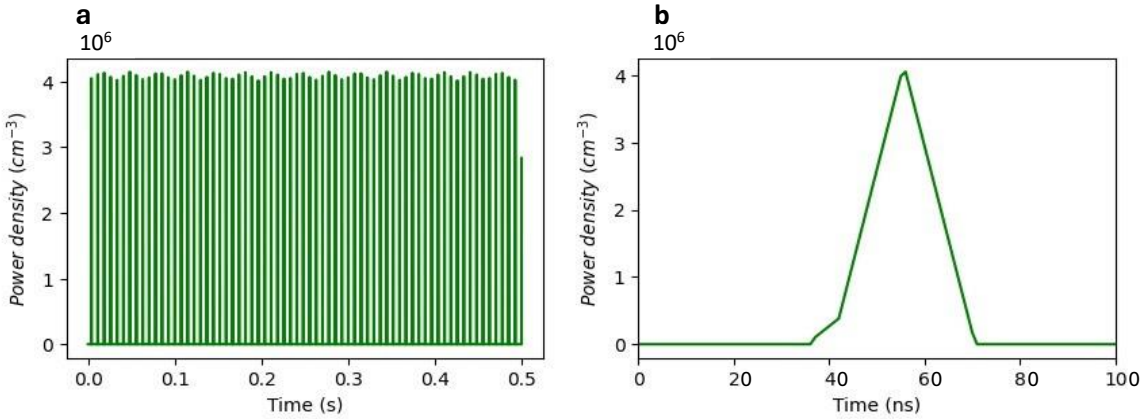

Figure 6. Pulsed power density profile (a) in the first 0.5s of the residence time and (b) on a shortened timescale to highlight each micro-discharge pulse.

The response of the reduced electric field and, consequently, that of the electron temperature to the power pulses is shown in Figure 7 and Figure 8, respectively. Similar to the power density, both profiles exhibit pulsed behaviour, and their peaks align in time with the power discharges, with an average peak value of ~ 400 Td for the reduced electric field and an average peak value of ~ 40,000 K (or ca. 3.447 eV) for the electron temperature. This alignment is anticipated since the model calculates the electric field based on the power input, which is then utilized for EEDF calculations and the determination of the electron temperature. The latter is crucial for assessing the energy of the electrons in the plasma zone, subsequently initiating chemical reactions with incoming CH_4 and NH_3 molecules in the gas flow.

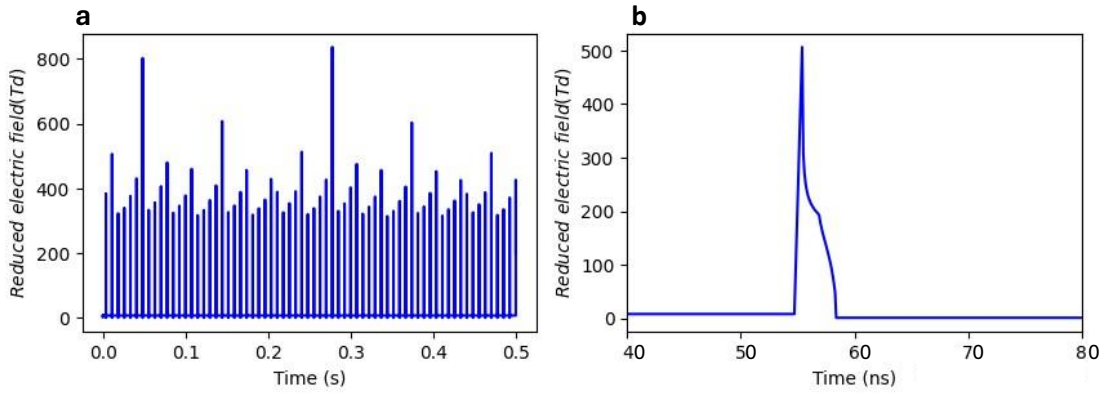

Figure 7. Reduced electric field profile (a) in the first 0.5s of the residence time and (b) on a shortened timescale to highlight each pulse.

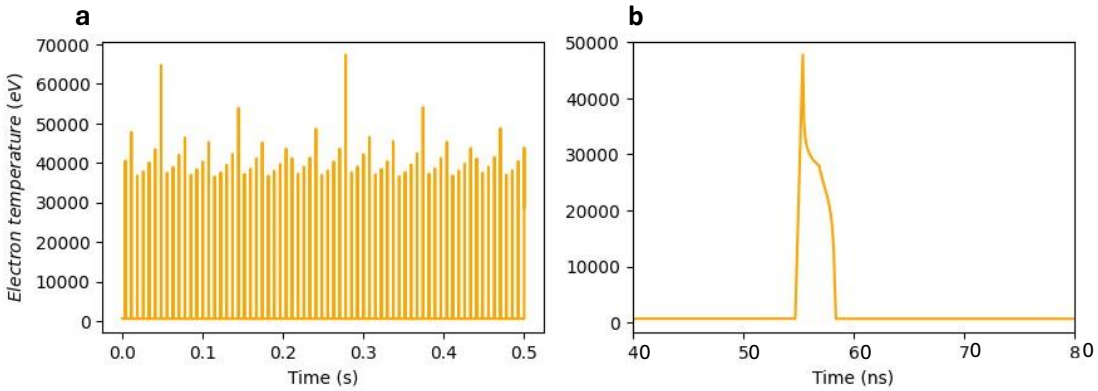

Figure 8. Electron temperature profile (a) in the first 0.5s of the residence time and (b) on a shortened timescale to highlight each pulse.

5.2 Modelled gas-phase kinetics

In this section, some results will be presented for the species of greatest interest, such as electrons, which play an important role during the micro-discharges by supporting the plasma discharge and participating in the collisional processes - leading to radicals, ions, excited species.

Then the density profiles of the reactants, CH_4 and NH_3, will be reported, with the most important formation and destruction reactions. Finally, the density profiles of the main products, C_2NH_3 and HCN, will be presented, for which the reactions of greatest interest for the formation and destruction are also listed and discussed in the dedicated section 5.2.2.

5.2.1 Electrons

Figure 9 shows the pulsed electron density profile over the first three pulses within the residence time. The importance of electrons is visible during the discharges, i.e. when their density reaches the highest values. The electron density along the entire residence time peaks at ~ 2.15 x 10^{14} cm^{-3} at the top of the power pulses. During the afterglows (i.e., the time between pulses), the electron density significantly decreases to ~ 10^9 cm^{-3}, which slows down or halts the electron impact processes, while recombination reactions become more significant due to the absence of electron impact.

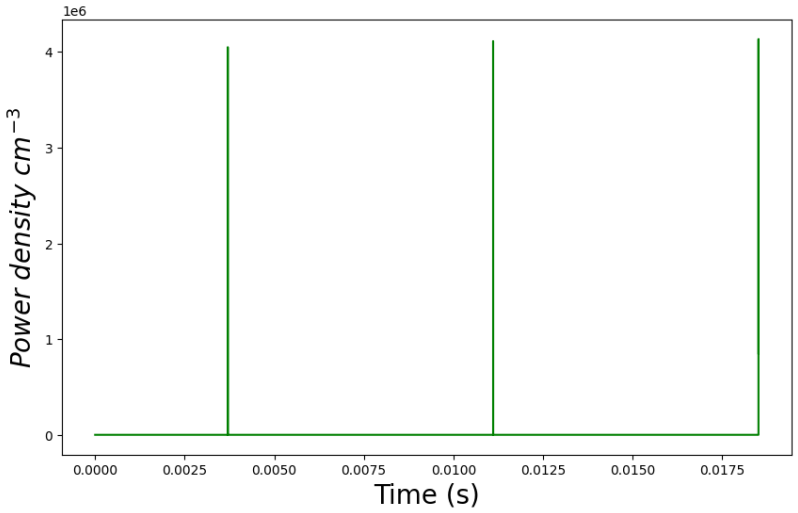

Figure 9.Electron density profile over the first three pulses within the residence time.

In Figure 10, the quasi-neutrality of the plasma is illustrated. The figure shows a clear overlap in the profiles of positive ions, negative ions, and electrons, indicating a charge equilibrium throughout the simulations. Initially, the charge density is in the order of 1.7 x 10^{14} cm^{-3}, and slightly increases over the residence time, but the difference between total positive ion and total negative densities is ~ 10^{9} – which is much lower than the charge density. We believe that this renders the simulations sufficiently quasi-neutral.

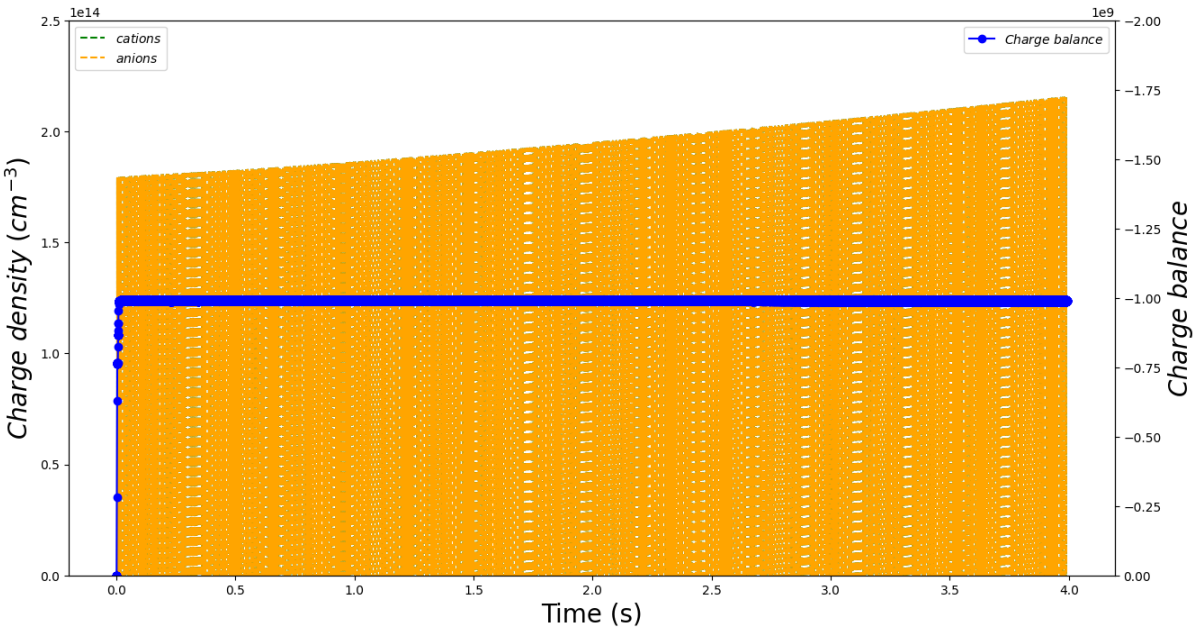

Figure 10. Density of sum of electrons and anions versus sum of cations (left y-axis), with the numerical difference shown on the right y-axis.

5.2.2 Feed gas molecules and major products

Figure 11 illustrates the density profiles of the species present in the initial gas mixture, CH_4 and NH_3, over the residence time. The observed trend aligns with the expected pattern of reactants, showing a gradual consumption of both CH_4 and NH_3 during the residence time.

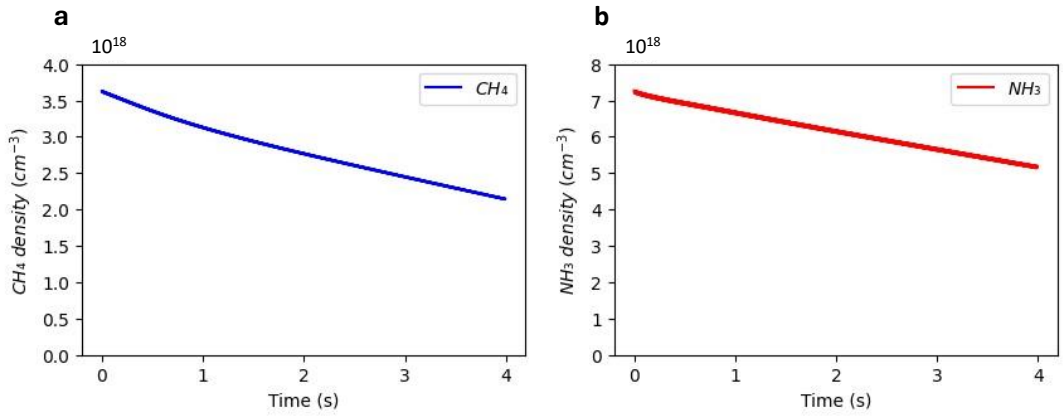

Figure 11. (a) CH_4 and (b) NH_3 density profiles over the residence time.

As can be seen in Figure 11, there is no plateau in the profiles at the end of the residence time, which means that steady state has not yet been reached in the residence time (~ 4 s), as the densities of the reagents continue to show a decreasing trend.

For a clearer insight in the behaviour of these species during the pulses and the afterglows, Figure 12 shows a zoomed in version of these profiles, where the timescale was reduced to ~0.02 seconds.

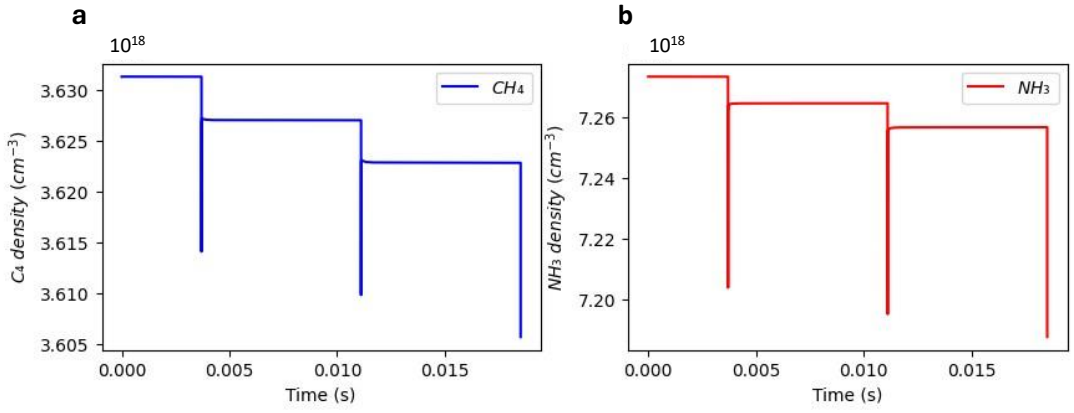

Figure 12. A zoom of (a) CH_4 and (b) NH_3 density profiles over the first 0.02 seconds of the residence time

Both reactants are mainly destroyed during the pulses through electron impact dissociation reactions, for methane: $e^- + CH_4 \rightarrow CH_3 + H + e^-$ (with a contribution of ~ 61%), $e^- + CH_4 \rightarrow CH_2 + H + H + e^-$ (~28%), $e^- + CH_4 \rightarrow CH_2 + H_2 + e^-$ (~ 7%). For ammonia the main electron impact

dissociation reaction is $e^- + NH_3 \rightarrow NH_2 + H + e^-$ (with a contribution of ~ 96%), and then $e^- + NH_3 \rightarrow NH + H_2 + e^-$ (~ 3%).

Subsequently, they are chiefly reformed during the afterglows through recombination reactions, mainly $CH_3 + H + M \rightarrow CH_4 + M$ (where M is any third body), $C_2NH_3 + CH_3 \rightarrow CH_4 + C_2NH_2$, $CH_3 + H_2 \rightarrow CH_4 + H$, with a contribution of ~ 88%, 6% and 4% for methane. For ammonia, the main formation reaction is $NH_2 + H + M \rightarrow NH_3 + M$ (which contributes with ~ 88%); followed by $CH_4 + NH_2 \rightarrow CH_3 + NH_3$ (~ 4%), and $H_2 + NH_2 \rightarrow NH_3 + H$ (~ 4%).

Figure 13 shows the density profile of the major products, HCN and C_2NH_3 and as expected, the trend is opposite to the profile of the reagents, illustrating a gradual production during the residence time.

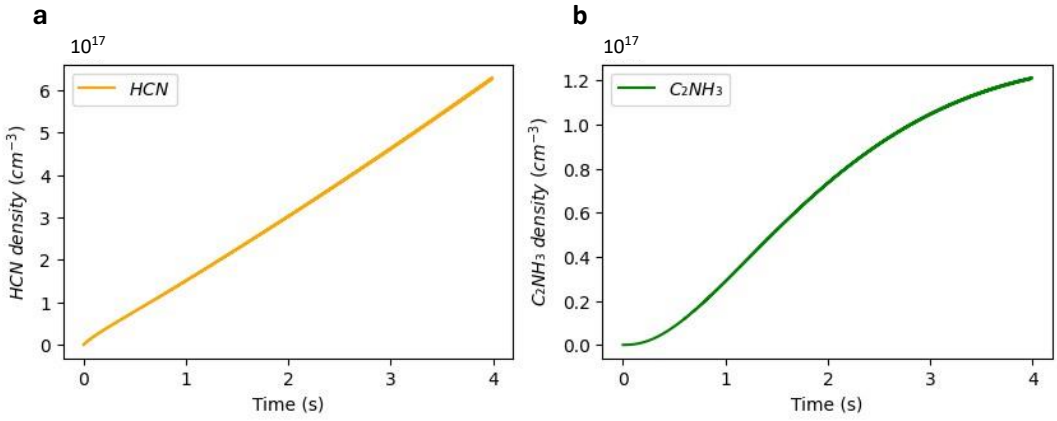

Figure 13.Density profiles of the main products (a) HCN and (b) C_2NH_3 over the residence time.

Figure 14 shows a zoom of the density profiles of the main products, which helps us to analyse the trend during the pulses and afterglows. In particular, it is noticeable that the formation takes place mainly during the micro discharges.

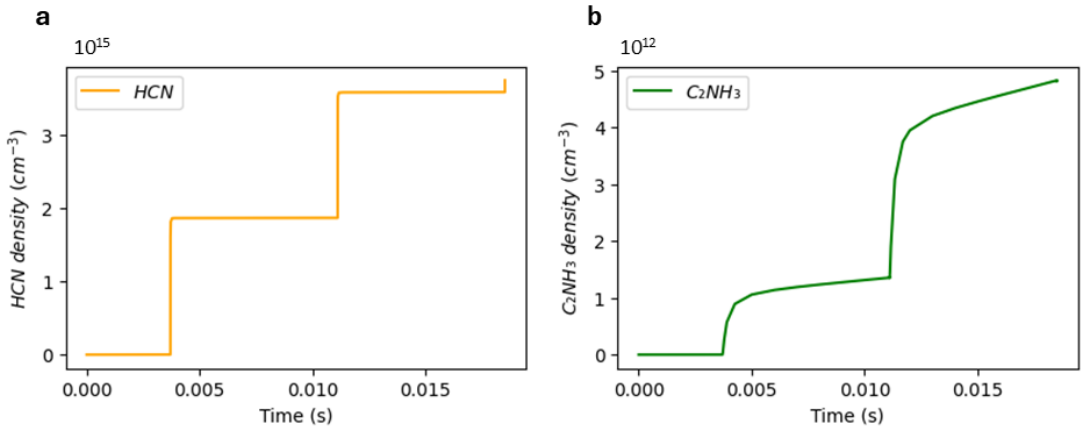

Figure 14. Density profiles as a function of time of (a) HCN and (b) C2NH3. The timescale was shortened to evidence the pulsed behaviour of these species during each micro-discharge and afterglow.

For HCN production, the reaction that plays the main role during the micro-discharges is $CH_3 + N \rightarrow HCN + H_2$ (~ 91%), whereas for C_2NH_3 production, two reactions play an important role: $C_2NH_2 + H + M \rightarrow C_2NH_3 + M$ (~ 63%) and $C_2NH_4 + H \rightarrow C_2NH_3 + H_2$ (~ 36%). It is also interesting to note that the formation of these products also occurs during the afterglows where in particular a greater formation of C_2NH_3 can be seen compared to HCN. The two main reactions being responsible for HCN formation: $CH_3 + N \rightarrow HCN + H_2$ (~46%) and $CNH_2 + NH_2 \rightarrow HCN+NH_3$ (~39%). Moreover, for C_2NH_3, the important formation reactions in the afterglows are $C_2NH_4 + H \rightarrow C_2NH_3 + H_2$ (~61%), $CN_2H_3 + CH_3 \rightarrow C_2NH_3 + NH_3$ (~27%) and $C_2NH_2 + H + M \rightarrow C_2NH_3 + M$ (~11%).

At the same time, the products are also partly being consumed again, both during the micro-discharges and afterglows. HCN is mainly consumed during the micro-discharges by ionisation: $e^- + HCN \rightarrow HCN^+ + e^-$ (~ 98%). This is the only electron impact reaction involving products in the model. During the afterglow, HCN is consumed through the reaction $HCN + CH_3 + M \rightarrow C_2NH_4 + M$ (~ 97%). As for C_2NH_3, during the micro-discharges, it is mainly consumed through the recombination reaction $H + C_2NH_3 + M \rightarrow C_2NH_4 + M$ (~ 90%), while during the afterglows, through $H + C_2NH_3 + M \rightarrow C_2NH_4 + M$ (~64%) and $C_2NH_3 + CH_3 \rightarrow CH_4 + C_2NH_2$ (~ 28%). It is important to note that electron impact dissociation reactions for HCN and C_2NH_3 are unfortunately not considered in the model, due to unavailability of such cross sections in the literature. While we are aware that these are important processes (given the high overall densities of these products), this is a current limitation of the model and future work plans to investigate this effect, possibly by assuming that these molecules have similar dissociation patterns to other molecules, with a calculated new threshold.

5.3 Modelled conversion and selectivity, and comparison against experimental results

In order to validate the modelled outputs against available experimental data, we have utilised the model to calculate conversion of the reactants and selectivity towards the main products. With the aim of validate the model in terms of CH_4 conversion and HCN and C_2NH_3 selectivity, we referred to the study by Yi et al., but as this study does not report any values for NH_3 conversion, for the validation in terms of NH_3 conversion we mainly referred to the experimental results reported by Bang et al. (as mentioned in section 2.4), obtained under conditions similar to those studied in our model.

The model results (blue bars) alongside a comparison with experimental data (orange bars) (3) (22) are shown in Figure 15.

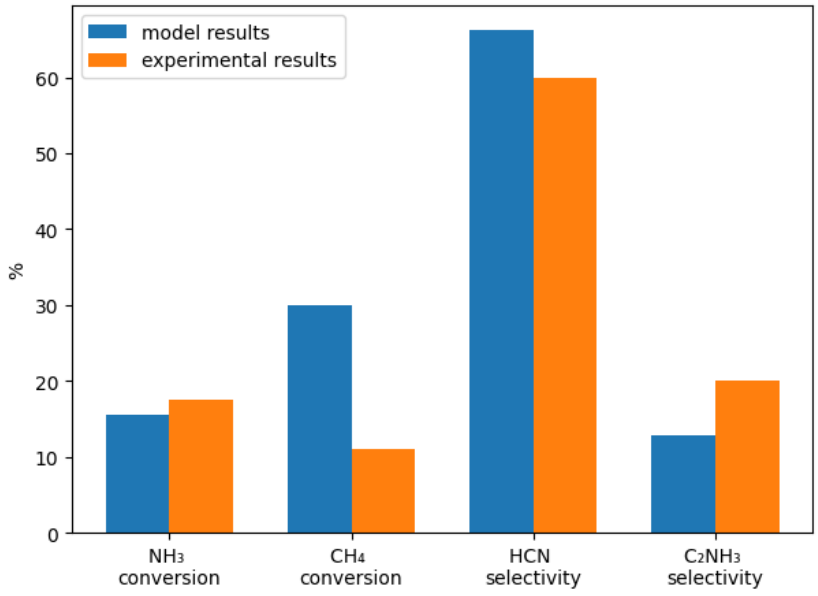

Figure 15. Comparison between model (blue bars) and experimental (orange bars) results, for NH_3 conversion from Bang et al. (22) and CH_4 conversion, HCN and C_2NH_3 selectivity from Yi et al. (3).

Looking at Figure 15, we note that the model predicts a conversion of CH_4 of about 30%, which is clearly overestimated compared to the experimental conversion obtained by Yi et al. (3), which was around 11.1%, and this could be due to multiple factors. The first reason could be that some conditions assumed in the model may be different from those in the experimental work, such as plasma volume, micro-discharge frequency, etc. Another reason could be the lack of rate coefficients for certain interactions between methane, ammonia and $C_xN_yH_z$ species. Table 5 below shows all the reactions in which, for the species listed in Table 4, some

assumptions were made, to compensate for this unavailability of data (as mentioned in section 4.2) and which includes CH_4 directly.

Table 5. Reactions present in the model chemical set that include $C_xN_yH_z$ or N_xH_y species assumed with similar reactivity as the corresponding $C_xO_yH_z$ or O_xH_y species and directly involving CH_4. The rate coefficients for these reactions were adopted from NIST database (28) based on the assumptions described in section 4.2.

$CH_4 + N_2H_3 \leftrightarrow CH_3 + N_2H_4$
$CH_3 + CNH_3 \rightarrow CH_4 + CNH_2$
$CH_3 + CNH_2 \rightarrow CH_4 + HCN$
$CH_3 + C_2NH_4 \rightarrow CH_4 + C_2NH_3$
$CH_3 + C_2NH_5 \leftrightarrow CH_4 + C_2NH_4$
$C_2NH_6 + H \rightarrow CH_4 + CNH_3$

The inclusion of these reactions with the hypothesis described in section 4.2, has allowed us to obtain the results shown in Figure 15, which although far from the experimental ones, represent the best investigated case. Surely to obtain a CH_4 conversion from the model that better approaches the experimental one represents the main objective for the future developments of this study.

The calculated results for selectivity of the HCN and C_2NH_3 products show a very good agreement with the results obtained experimentally by Yi et al. (3). In their experiments, the selectivity of HCN was around 60%, while the calculated one is only slightly overestimated, i.e., around 66%. Vice versa, the experimental selectivity of C_2NH_3 was around 20%, while the modelled selectivity is about 12-13%; thus, slightly underestimated. This discrepancy with the experimental values obtained by Yi et al. (3), may be due to some initial conditions set differently, because not all input values needed for the model (like number of micro-discharges, pulse frequency and duration,…) were reported in the experimental study. Or, as mentioned above, it could be due to the lack of data on the rate coefficients for interactions between CH and NH species or again the unavailability of electron impact cross section data for the dissociation of both these products. As mentioned already, the non-availability of this data is, from our point of view, the main reason why the results of the model deviate from the

experimental ones. The availability of such data or the possibility to make some other hypotheses in order to compensate such lack, represents one of the successive steps to investigate in order to improve the model here introduced.

Finally, according to Bang (22), within a temperature range of 600-700 K, at atmospheric pressure and a total discharge power of 20 W, the conversion of NH_3 lies in the range of 15-20%. Therefore, as the modelled NH_3 conversion (15.5%) is in line with Bang's observations, we believe that this conversion must be reasonably accurate in the framework of this thesis. This is corroborated by the good agreement observed in the selectivity results, which are directly related to initial and final densities of NH_3.

No other experimental examples with similar conditions were found in the literature to further validate the modelled NH_3 conversion. While there are many studies on the decomposition of ammonia to produce H_2, most of these use plasma-catalytic processes, investigating different types of catalysts in order to achieve the desired results. Therefore, it is challenging to validate the conversion of NH_3 modelled, due to difficulties in comparing the results of this model with those reported in the above-mentioned studies. Indeed, the NH_3 conversion varies greatly across these studies and the conditions are not comparable with those modelled here.

Still in terms of selectivity, Table 6 shows the products that exceed 0.8% selectivity in the model.

Table 6. Products exceeding 0.8% selectivity (except HCN and C2NH3)

C_2H_6	2.0%
C_3H_8	1.1%
N_2H_3	0.8%
C_2NH_5	0.9%
CN_2N_4	0.8%

The only species exceeding 0.8% selectivity in the model are C_2H_6, C_3H_8, N_2H_3, C_2NH_5 and CN_2N_4 (except HCN and C_2NH_3), however they have selectivity equal or below 2%. The results just commented find the same feedback also in the work of Yi et al. (3). Indeed, even in his work,

Yi et al. do not note such selectivity as to be relevant for these products. Moreover, both from the results obtained with the model and from those observed experimentally, we can say that, for this type of chemistry and this type of gas concentration, although the formation of hydrocarbons during the process is considerable, they tend to react and be consumed quite rapidly for the formation of $C_xN_yH_z$ compounds. Thus, as the model does not record any significant hydrocarbon selectivity, the suggestion from the experimental results is corroborated here. From the table, one can see the N_2H_3 selectivity (low but comparable with the others), which, together with N_2H_4 species, represents an important radical in the chemistry of plasma-assisted ammonia decomposition (as pointed out in Bang's study (22)) and, as we shall see in the following sections, also in the chemistry involving CH_4 and NH_3.

This analysis will be elaborated extensively in section 5.4, where the reaction pathway results obtained from the model are discussed.

5.4 Reaction pathway analysis

The formation and consumption mechanisms of all important species were investigated by conducting time-resolved calculations for the reaction rates of all processes incorporated in the model, both during the micro-discharge pulses and their afterglows. A comprehensive diagram was created, illustrating the reaction pathways for the most prevalent reactants and products in the model. The findings are depicted in Figure 16 (which showcases the primary reaction pathways of neutral species) and discussed below.

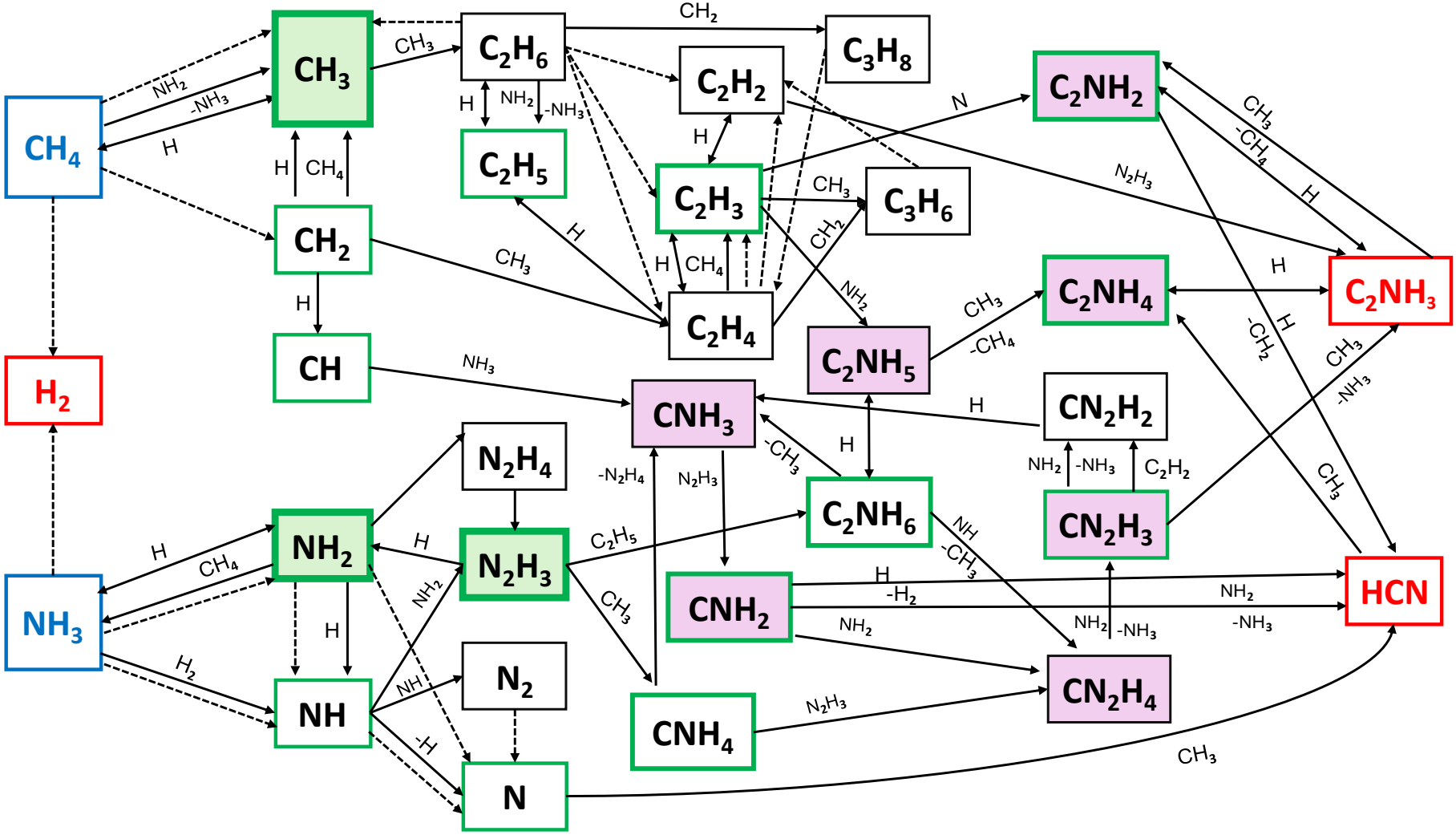

Figure 16. The complex network of molecules and reactions involved in the conversion of (33.3%) CH_4 and (66.7%) NH_3. In the blue boxes are the reactants. In the green boxes are the radicals, with the boxes with green coloured background showing the most important ones. In the red boxes are the main products. And finally, in the black boxes are the other stable molecules. Furthermore, in the boxes with purple background are the most important $C_xN_yH_z$ species leading to the main products. The double-arrow lines in the diagram indicate reactions occurring in both directions. The dashed arrows indicate electron impact dissociation. Recombination reactions are indicated with solid simple arrows. H radicals are not shown but they are the most abundant radicals in the model, participating in many reactions.

5.4.1 Ammonia (NH_3) and decomposition products (NH_2 and NH)

One of the most abundant molecules in the model is clearly NH_3, comprising 66.6% of the initial gas mixture. During the micro-discharges, when the electron density reaches its peak, NH_3 dissociates by electron impact into its two radicals NH_2 (95%) and NH (3%) (see Figure 16). The formation of one of the major products of the process, i.e. H_2 (54%), also occurs via electron impact dissociation of NH_3 during the micro-discharges (see also Figure 16). In the afterglows, the NH_2 radical tends to recombine with H (88%) and H_2 (4%) into ammonia again; but it also reacts with methane, giving rise to again NH_3 and the CH_3 radical (4%), of which the formation/destruction will be discussed below. During the micro-discharges, the two radicals NH and NH_2 also undergo electron impact dissociation, leading to the formation of N radicals (79% by NH_2 and 18% by NH). The latter is completely consumed (99%) through its interaction with CH_3 forming directly HCN (see Figure 16).

5.4.2 N_xH_y species

Still during the micro-discharges, the interaction between two NH_2 radicals forms N_2H_4 (99%) which in turn loses an H atom and is completely (~100%) consumed to form the radical N_2H_3. This radical is extremely important for the formation of various intermediates, such as CNH_4 and C_2NH_6, that lead to the formation of acetonitrile (C_2NH_3). N_2H_3 is also formed by the recombination reaction of the radicals NH_2 and NH with a contribution of 13%.

5.4.3 Methane (CH_4)

Another important molecule present is methane, which accounts for 33.3% of the inlet gas mixture. Due to the high electron density and high electron temperature during the micro-discharges, methane dissociates by electronic impact reactions into CH_3 (62%) and CH_2 (36%). As soon as the electron density drops in the afterglows, the CH_3 radical recombines with H (89%) and H_2 (3%), again forming CH_4; while the CH_2 radical reacts with H (41%) to form H_2 and the CH radical. The CH radical recombines with NH_3, into the formation of the stable species CNH_3 (with a contribution of 98%), as will be discussed later.

5.4.4 C_xH_y species

Hydrocarbons, like C_2H_x, are formed through recombination reactions between primary CH_x radicals. In particular, the C_2H_6 molecule is mainly formed via recombination between two CH_3

radicals, both during the micro-discharges (27%) and the afterglows (72%). This molecule leads to the formation of C_2H_4 by electron impact dissociation (35%). C_2H_6 and C_2H_4 contribute to the formation of C_2H_2, with a contribution of 29% by C_2H_6 and 22% by C_2H_4. C_2H_2 in turn leads directly to the production of C_2NH_3 upon reaction with N_2H_3 (with a contribution of 16% during the afterglows).

Furthermore, the recombination reaction between C_2H_4 and H, either during the micro-discharges (76%) and the afterglows (59%), leads to the formation of C_2H_5. This is also an important radical since it reacts with N_2H_3 into C_2NH_6 (9%) radicals, which will be discussed below. Note that there is no arrow from C_2H_5 to C_2NH_6 in Figure 16, to not make the figure even more busy; but C_2H_5 is indicated as reactant (next to the arrow) from N_2H_3 to C_2NH_6.

The C_2H_3 radical is formed during the micro-discharges through electron impact dissociation of C_2H_4 (39%) and C_2H_6 (15%) and by recombination of C_2H_2 with H (38%). During the afterglows, C_2H_3 recombines with N to form the C_2NH_2 radical (72%).

5.4.5 CNH_y species

The CNH_3 radical, already presented in the methane section (5.4.3), is completely consumed (99%) both in the micro-discharges and the afterglows to form CNH_2. This radical can recombine with H (6%) and with NH_2 (71%) to form HCN. In addition, its recombination with NH_2 (8%) could also lead to the formation of CN_2H_4, an important molecule that will be discussed in the next section.

5.4.6 C_2NH_y and CN_2H_y species

C_2NH_2 is consumed both during the micro-discharges and the afterglows, by recombination with H. This interaction can give rise to two different scenarios, the first with production of C_2NH_3 (with a contribution of 60%) and the second with formation of HCN (with a contribution of 40%).

In addition to the above section, the C_2NH_6 radical is mainly formed (90%) upon recombination (both in the micro-discharges and afterglows) of C_2NH_5 with H, but it is also mainly consumed (with a contribution of 67% during the micro-discharges and 89% in the afterglows) through a dissociation reaction that results in the formation of C_2NH_5 molecule.

C_2NH_5 is one of the most important molecules in this chemistry. On the one hand, C_2NH_5 reacts with the CH_3 radical into C_2NH_4 (7%), which in turn loses an H atom during both the micro-discharges (99%) and afterglows (99%), forming one of the major products C_2NH_3. On the other hand, it tends to bind to H_2, both during the micro-discharges (99%) and afterglows (89%), giving rise again to the C_2NH_6 radical, which subsequently, upon reaction with the NH radical, participates in the formation of the CN_2H_x species, such as CN_2H_4, with a contribution of 94% during the micro-discharges and 79% during the afterglows. The stable molecule CN_2H_4 is totally consumed, both during the micro-discharges and afterglows (99%), through recombination with the radical NH_2 forming CN_2H_3. The radical CN_2H_3 leads to the direct formation of C_2NH_3 upon recombination with CH_3, both during the micro-discharges (19%) and afterglows (68%).

5.4.7 Main products: HCN and C_2NH_3

The reactions of most importance in the formation of the main products are shown separately in Figure 17. This representation allows us to visualise more immediately the molecules and radicals directly involved and their relative contribution in %, both during the micro-discharges and the afterglows.

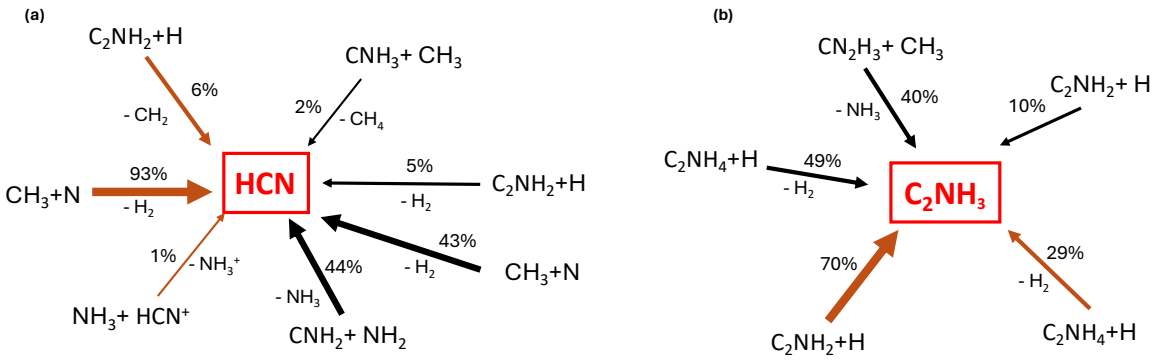

Figure 17. Main reaction pathways leading to the formation of (a) HCN and (b) C_2NH_3 in our model. The contribution of each formation pathway is indicated with arrows of different thickness depending on the percentage with which they contribute to the formation of each product. Brown arrows indicate reactions occurring during the micro-discharges while black arrows represent the ones occurring in the afterglows.

Figure 17 clearly indicates that the radicals CNH_2, C_2NH_2, C_2NH_4 and CN_2H_3, upon recombination with methane, ammonia and H radicals, have a determining role in the formation of both products, either during the micro-discharges and in the afterglows. In the case of HCN, a fundamental role in its formation is given by the recombination between CH_3 and N. This reaction represents the main pathway for the production of HCN in this model, with a contribution of 93% during the micro-discharges and 43% in the afterglows, when the

CNH_2 radical also recombines with NH_2 and contributes with 44% to the formation of HCN. In contrast, the two radicals C_2NH_2 and C_2NH_4, through recombination reactions with H, play a decisive role in the formation of C_2NH_3. During the micro-discharges, C_2NH_2 contributes with 70% and C_2NH_4 with 29%. During the afterglows, the former contributes with 10% and the latter with 49%, and in fact, in this case the CN_2H_3 radical also participates with a contribution of 40%.

In summary, it is clear that the production of HCN and C_2NH_3 from NH_3 and CH_4 is quite complex, and proceeds through several steps, involving CNH_x and C_2NH_x radicals. Of course, this reaction mechanism is only based on our model, and not validated by experiments, because the intermediate species are difficult to measure (and/or were not reported in the only experimental paper available). However, as the calculated product selectivities are in reasonable agreement with the experiments, we believe the reaction mechanism should also be realistic. Furthermore, this shows the advantage of modelling: to gain insight in the underlying mechanisms, which is not straightforward by experiments.

6 Conclusion

In this thesis, the ammonia reforming of methane to produce hydrogen cyanide (HCN) was studied using a 0D plasma kinetic model, which performed time-resolved calculations of species densities and incorporates reaction rate coefficients dependent on gas temperature and pressure. Some measured experimental conditions in the work by Yi et al. (3), such as 673 K gas temperature, 1 bar pressure, and approximately 4 s of residence time, were adopted as input for the model. The simulation results exhibited pulsed behaviour for all plasma parameters, including the reduced electric field, power density, and plasma species densities, such as electron density, which is logical, as it results from the "pulsed behaviour" of the micro-discharge filaments.

This was validated against experimental results from a DBD plasma reactor utilised by Yi et al. (3) to study ammonia reforming of methane. A good agreement was observed with the experimental measurements of the selectivity of both the main products, HCN and C_2NH_3. These important results suggest that the kinetic dynamics of the gas phase occurring in the reactor are comparable to those included in the model. Additionally, a good conversion of NH_3 was validated, considering mainly the work of Bang et al. (22), whose conditions are closer to those of the case study of this thesis. However, the model overestimated the conversion of CH_4 compared to the experimental results.

Analysis of the reaction pathways from the simulation results reveals that the mechanisms responsible for the formation of different products involve CH_3, N, NH_2, N_2H_3, H radicals with CNH_2, C_2NH_2, C_2NH_4, CN_2H_3 radicals. Among them, the most important radicals that have a higher modelled density than the others are N_2H_3, CN_2H_3 and C_2NH_2. The analysis of the processes that lead to the formation of products highlights the complexity of the interactions between the different plasma species in a system of this type.

Modelling the plasma-chemical process described in this paper can be the starting point for understanding the complexity of the chemistry involving CH_4 and NH_3, as well as for obtaining practical information to understand and predict the plasma dynamics. Certainly, a big step towards improving this model would be the possibility of obtaining rate coefficient data currently unavailable in the literature. In the future, it would also be interesting to investigate the effect of other parameters not expressed in the experimental reference case, such as

plasma volume, discharge frequency or with a different type of plasma, in order to hopefully find a value for CH_4 conversion that is more consistent with the experimental one and probably to improve the efficiency of technological applications based on this type of process.

7 Bibliography

1. *Handbook of Heterogeneous Catalysis.* Ertl, G., Knözinger, H.; Schüth, F.; Weitkamp, J. 2008. 9783527610044.

2. *Electrify to decarbonize. Uschbe B.*, 2023, Nature Catalysis, Vol. 6, p. 1099-1100.

3. *Plasma-Catalytic Ammonia Reforming of Methane over Cu-Based Catalysts for the Production of HCN and H2 at Reduced Temperature.* Yanhui Yi, Xin Wang, Amin Jafarzadeh, Li Wang, Pei Liu, Bowen He, Jinhui Yan, Rui Zhang, Hantian Zhang, Xi Liu, Hongchen Guo, Erik C. Neyts, and Annemie Bogaerts. 3, 2021, Vol. 11, p. 1765–1773.

4. *Proton conduction enabled highly selective acetonitrile detection at moderate operating temperature by using Ag-decorated sodium titanate nanoribbons.* Fengshuang Zheng, Fengpan Ma, Lubing Cai, Xuemin Zhang. 2024, Journal of Molecular Liquids, Vol. 395, p. 123843. 0167-7322.

5. *Gas Sensing for Industrial Relevant Nitrogen-containing Compounds Using a Microelectronics-Based Absorption Spectrometer in the 220–330 GHz Frequency Range.* Timothy E. Rice, M. Arshad Zahangir Chowdhury, Megan N. Powers, Muhammad Waleed Mansha, Ingrid Wilke, Mona M. Hella, Matthew A. Oehlschlaeger. Sensors and Actuators B: Chemical, 2022, Vol. 367, p. 132030. 0925-4005.

6. *Low-pressure hydrogen plasmas explored using a global model. 2015* Corr, Cameron M Samuell and Cormac S., Plasma Sources Science and Technology, Vol. 25.

7. *A Short Introduction to Plasma Physics.* Wiesemann, K. Germany, 2014.

8. *Plasma chemistry and kinetics in a magnetized hydrogen plasma expansion : a study of negative ions.* W.E.N. Harskamp, 2012, *Applied Physics and Science Education.*

9. Kinetic and Diagnostic Studies of Molecular Plasmas Using Laser Absorption Techniques. S Welzel, A Rousseau, P B Davies and J Röpcke. 2007, Journal of Physics D: Applied Physics, Vol. 49, p. 243001. 978-3-642-10591-3.

10. Surface modification of recycled polymers in comparison to virgin polymers using Ar/O2 plasma etching. Marion Höhener, Patrick Rupper, Barbara Hanselmann, Rudolf Hufenus, Sandro Lehner, Edith Perret, Dirk Hegemann. 2022, Vol. 19, p. 2200068.

11. Non-equilibrium in low-temperature plasmas. Taccogna, F., Dilecce, G., 2016, Eur. Phys. J. D, Vol. 70.

12. Vibrational Kinetics, electron dynamics and elementary processes in H2 and D2 Plasmas for Negative Ion Production: Modelling Aspects. M. Capitelli, M. Cacciatore, R. Celiberto, O. D. Pascale, P. Diomede, F. Esposito, A. Gicquel, C. Gorse, K. Hassouni, A. Laricchiuta, S. Longo, D. Pagano, M. Rutigliano. 2006, Nucl. Fusion, Vol. 46.

13. From ozone generators to flat television screens: history and future potential of dielectric-barrier discharges. Kogelschatz U, Eliasson B and Egli W. 1999, Pure and Applied Chemistry, Vol. 71, p. 1819-1828.

14. Reaction kinetic modelling of tar cracking in a non-thermal plasma reactor: Model evaluation and reaction mechanism investigation. Eric Sanjaya, Gustavo Weihs, Norhuda Abdul Manaf, Ali Abbas. 2023, Chemical Engineering Journal, Vol. 479. 1385-8947.

15. A chemical kinetics simulation of plasma-catalytic dry reforming. Shengfei Wang, Vandad Rohani, Paul Dupont, Sylvain Pagnon, Laurent Fulcheri. 2023, Chemical Physics, Vol. 574. 0301-0104.

16. Plasma activation of CO2 in a dielectric barrier discharge: A chemical kinetic model from the microdischarge to the reactor scales. Martin Alliati, Danhua Mei, Xin Tu. 2018, Journal of CO2 Utilization, Vol. 27, p. 308-319. 2212-9820.

17. ZDPlasKin-Zero-Dimensional Plasma Kinetics solver. S. Pancheshnyi, B. Eismann, G.J.M. Hagelaar, L.C. Pitchford. [Online] University of Toulouse, LAPLACE, CNRS-UPS-INP, Toulouse, France, 2008. http://www.zdplaskin.laplace.univ-tlse.fr.

18. Zero-dimensional modeling of unpacked and packed bed dielectric barrier discharges: the role of vibrational kinetics in ammonia synthesis. K van ‘t Veer, F Reniers, A Bogaerts. 2020, Plasma Sources Science and Technology.

19. The LXCat project: Electron scattering cross sections and swarm parameters for low temperature plasma modeling Chemical Physics. Pancheshnyi S., Biagi S., Bordage M.C., Hagelaar G.J.., Morgan W.L., Phelps A.V., Pitchford L.C. 2012.

20. Methane coupling in nanosecond pulsed plasmas: Correlation between temperature and pressure and effects on product selectivity. Eduardo Morais, Evangelos Delikonstantis, Marco Scapinello, Gregory Smith, Georgios D. Stefanidis, Annemie Bogaerts. 142227, 2023 : s.n., Chemical Engineering Journal, Vol. 462. 1385-8947.

21. Ammonia decomposition in a dielectric barrier discharge plasma: Insights from experiments and kinetic modeling. J.A. Andersen, K. van 't Veer, J.M. Christensen, M. Østberg, A. Bogaerts, A.D. Jensen. 2022, Chemical Engineering Science, Vol. 271. 0009-2509.

22. Kinetic Study for Plasma Assisted Cracking of NH3: Approaches and Challenges. Seunghwan Bang, Ramses Snoeckx, and Min Suk Cha. 5, s.l. : J. Phys. Chem. A, 2023, Vol. 127, p. 271−1282.

23. Hagelaar, Gerjan. BOLSIG+ - Electron Boltzmann equation solver. [Online] LAPLACE laboratory in Toulouse in France. https://www.bolsig.laplace.univ-tlse.fr/index.html.

24. University of Toulouse, LAPLACE, CNRS-UPS-INP, France; ABB Corporate Research, Switzerland. ZDPLASKIN Zero-Dimensional Plasma Kinetics solver. Manual. [Online] 2016. http://www.zdplaskin.laplace.univ-tlse.fr/index.html.

25. Cross Sections for Electron Collisions with Methane. Song, Mi-Young, 2015. 023101, J. Phys. Chem., vol. 44.

26. Hayashi, database. LXCat. [Online] www.lxcat.net/Hayashi..

27. Evaluated Kinetic Data for Combustion Modeling: Supplement II. D. L. Baulch, C. T. Bowman, C. J. Cobos, R. A. Cox, Th. Just, J. A. Kerr, M. J. Pilling, D. Stocker, J. Troe, W. Tsang, R. W. Walker, J. Warnatz. 3, 2005, J. Phys. Chem. Ref. Data, Vol. 34.

28. NIST Chemical Kinetics Database. Kinetics Database Resources. [Online] https://kinetics.nist.gov/kinetics/index.jsp.

29. The UMIST Database for Astrochemistry. [Online] http://udfa.ajmarkwick.net/.

30. Plasma-based CO2 conversion: How to correctly analyze the performance? 2023, Journal of Energy Chemistry, Vol. 86, p. 180-196.

31. Plasma-based CO2 conversion: How to correctly analyze the performance?. Bart Wanten, Rani Vertongen, Robin De Meyer, Annemie Bogaerts. 2023, Journal of Energy Chemistry, Vol. 86, p. 180-196.

8 Appendix

Table 1. Overview of the different reactions included in the non-thermal CH_4/NH_3 reaction mechanism, with references where the reactions and rate coefficients were adopted from. The reaction rate coefficients are in the Arrhenius form: $k = A \times T_{gas}^{n} \times e^{(-Ea)/(Rgas \times Tgas),}$ in $cm^3/(molecule\ s)$ for 2-body reactions, in $cm^6/(molecule^2\ s)$ for 3-body ones.

With the symbol:

(*) → reactions for which we have assumed a similar reactivity as for the analogous oxygen molecules for the species indicated in section 4.2 .

(**) → reactions with a calculated inverse reaction rate coefficient using detailed balancing from Slaets et al. (6).

$H + NH_3 \rightarrow NH_2 + H_2$	$8.4x10^{-14} * \left(\frac{T_{gas}}{300}\right)^{4.1} * e\left(-\frac{4760}{T_{gas}}\right)$	(1)
$NH_3 + NH \rightarrow NH_2 + NH_2$	$2.33x10^{-14} * \left(\frac{T_{gas}}{298.0}\right)^{3.41} * e\left(-\frac{7350.0}{T_{gas}}\right)$	(1)
$NH_3 + M \rightarrow H_2 + NH + M$	$1.05x10^{-9} * e\left(-\frac{47029.0}{T_{gas}}\right)$	(1)
$NH + NH_2 \rightarrow NH_3 + N$	$1.66x10^{-12}$	(1)
$H_2 + NH_2 \rightarrow NH_3 + H$	$5.4x10^{-11} * e\left(-\frac{6492}{T_{gas}}\right)$	(1)
$H + NH_2 + N_2 \rightarrow NH_3 + N_2$	$\left(\frac{1.0}{380}\right) * 5.5x10^{-30}$	(1)
$H + NH_2 + H_2 \rightarrow NH_3 + H_2$	$\left(\frac{1.0}{380}\right) * 5.5x10^{-30}$	(1)
$NH + H_2 + N_2 \rightarrow NH_3 + N_2$	$\left(\frac{1.0}{380}\right) * 2.5x10^{-35} * \left(\frac{T_{gas}}{300}\right) * e\left(\frac{1700}{T_{gas}}\right)$	(1)
$NH + H_2 + H_2 \rightarrow NH_3 + H_2$	$\left(\frac{1.0}{380}\right) * 2.5x10^{-35} * \left(\frac{T_{gas}}{300}\right) * e\left(\frac{1700}{T_{gas}}\right)$	(1)
$NH_2 + NH_2 \rightarrow NH_3 + NH$	$5.07x10^{-15} * \left(\frac{T_{gas}}{298.0}\right)^{3.53} * e\left(-\frac{278.0}{T_{gas}}\right)$	(1)
$H + NH_2 \rightarrow H_2 + NH$	$6.6x10^{-11} * e\left(-\frac{1840}{T_{gas}}\right)$	(1)

$N + NH_2 \rightarrow N_2 + H + H$	$1.2x10^{-10}$	(1)
$NH_2 + N \rightarrow NH + NH$	$2.99x10^{-13} * e\left(-\frac{7600.0}{T_{gas}}\right)$	(1)
$NH_2 + M \rightarrow H + NH + M$	$1.99x10^{-9} * e\left(-\frac{38248.0}{T_{gas}}\right)$	(1)
$NH + NH \rightarrow N + NH_2$	$1.7x10^{-12} * \left(\frac{T_{gas}}{300}\right)^{1.5}$	(1)
$H + NH + N_2 \rightarrow NH_2 + N_2$	$\left(\frac{1.0}{380}\right) * 1.0x10^{-32}$	(1)
$H + NH + H_2 \rightarrow NH_2 + H_2$	$\left(\frac{1.0}{380}\right) * 1.0x10^{-32}$	(1)
$N(2D) + NH_3 \rightarrow NH + NH_2$	$1.1x10^{-10}$	(1)
$H_2 + NH \rightarrow H + NH_2$	$3.50x10^{-11} * e\left(-\frac{7758.0}{T_{gas}}\right)$	(1)
$N + NH \rightarrow H + N_2$	$5x10^{-11}$	(1)
$H + NH \rightarrow N + H_2$	$5.4x10^{-11} * e\left(-\frac{165}{T_{gas}}\right)$	(1)
$NH + NH \rightarrow H_2 + N_2$	$5x10^{-14} * \left(\frac{T_{gas}}{300}\right)$	(1)
$NH + NH \rightarrow N_2 + H + H$	$8.5x10^{-11}$	(1)
$N + NH \rightarrow H + N + N$	$4.02x10^{-10} * \left(\frac{T_{gas}}{298.0}\right)^{-0.20} * e\left(-\frac{27303.0}{T_{gas}}\right)$	(1)
$NH + M \rightarrow H + N + M$	$2.99x10^{-10} * e\left(-\frac{37647.0}{T_{gas}}\right)$	(1)
$H + N + N_2 \rightarrow NH + N_2$	$\left(\frac{1.0}{380}\right) * 1.0x10^{-33}$	(1)

$N(\,_2D) + H_2 \rightarrow H + NH$	$2.3x10^{-12}$	(1)
$N(\,_2P) + H_2 \rightarrow H + NH$	$2.5x10^{-14}$	(1)
$N_2 + H \rightarrow NH + N$	$5.27x10^{-10} * \left(\frac{T_{gas}}{298.0}\right)^{0.50} * e\left(-\frac{74453.0}{T_{gas}}\right)$	(1)
$N_2 + M \rightarrow N + N + M$	$8.37x10^{-4} * \left(\frac{T_{gas}}{298}\right)^{-3.50} * e\left(-\frac{113710}{T_{gas}}\right)$	(1)
$N + N + M \rightarrow N_2 + M$	$1.38x10^{-33} * e\left(\frac{502.978}{T_{gas}}\right)$	(1)
$N(\,_2P) + N_2 \rightarrow N + N_2$	$2.0x10^{-18}$	(1)
$N + N + H_2 \rightarrow N_2 + H_2$	$\left(\frac{1.0}{380}\right) * 8.3x10^{-34} * e\left(\frac{500}{T_{gas}}\right)$	(1)
$H + H + N_2 \rightarrow H_2 + N_2$	$\left(\frac{1.0}{380}\right) * 8.3x10^{-33} * \left(\frac{300}{T_{gas}}\right)$	(1)
$H_2 + N_2 \rightarrow H + H + N_2$	$2.61x10^{-8} * \left(\frac{T_{gas}}{298.0}\right)^{-1.40} * e\left(-\frac{52561.0}{T_{gas}}\right)$	(1)
$N(\,_2D) + N_2 \rightarrow N + N_2$	$2.3x10^{-14} * e\left(-\frac{510.0}{T_{gas}}\right)$	(1)
$N(\,_2P) + N \rightarrow N + N$	$1.8x10^{-12}$	(1)
$N(\,_2P) + M \rightarrow N + M$	$2.4x10^{-14}$	(1)
$N(\,_2P) + N \rightarrow N(\,_2D) + N$	$6.0x10^{-13}$	(1)
$N^+ + CH_4 \rightarrow HCN^+ + H_2 + H$	$5.60x10^{-11}$	(3)
$H^{2+} + CN \rightarrow HCN^+ + H$	$1.20x10^{-9} * \left(\frac{T_{gas}}{300}\right)^{-0.50}$	(3)

$H^{3+} + CN \rightarrow HCN^{+} + H_2$	$2.00x10^{-9} * \left(\frac{T_{gas}}{300}\right)^{-0.50}$	(3)
$H + HCN^{+} \rightarrow HCN + H^{+}$	$3.70x10^{-11}$	(3)
$CH_2 + HCN^{+} \rightarrow CN + CH^{3+}$	$8.70x10^{-10}$	(3)
$NH + HCN^{+} \rightarrow CN + NH^{2+}$	$6.50x10^{-10} * \left(\frac{T_{gas}}{300}\right)^{-0.50}$	(3)
$C + N_2 \rightarrow CN2$	$3.09x10^{-33}$	(2)
$C + N_2 \rightarrow CN + N$	$8.70x10^{-11} * e\left(-\frac{188000.0}{R_{gas} * T_{gas}}\right)$	(2)
$N_2 + C2 \rightarrow CN + CN$	$2.49x10^{-11} * e\left(-\frac{175000.0}{R_{gas} * T_{gas}}\right)$	(2)
$CH + N_2 \rightarrow HCN + N$	$1.99x10^{-13} * \left(\frac{T_{gas}}{298}\right)^{1.42} * e\left(-\frac{86470.0}{R_{gas} * T_{gas}}\right)$	(2)
$N_2 + CH_2 \rightarrow HCN + NH$	$8.00x10^{-12} * e\left(-\frac{150000.0}{R_{gas} * T_{gas}}\right)$	(2)
$C + N \rightarrow CN$	$9.40x10^{-33}$	(2)
$CH + N \rightarrow C + NH$	$3.02x10^{-11} * \left(\frac{T_{gas}}{298}\right)^{0.65} * e\left(-\frac{10060.0}{R_{gas} * T_{gas}}\right)$	(2)
$CH + N \rightarrow CN + H$	$1.10x10^{-10}$	(2)
$N\left({}_2D\right) + CH \rightarrow CN + H$	$2.70x10^{-10}$	(2)
$N + CH_2 \rightarrow CNH_2$	$1.30x10^{-10}$	(2)
$N + CH_2 \rightarrow CH + NH$	$9.96x10^{-13} * e\left(-\frac{170000.0}{R_{gas} * T_{gas}}\right)$	(2)

$N(\,_2D) + CH_2 \rightarrow CNH_2$	$2.70x10^{-10}$	(2)
$CH_3 + N \rightarrow H + CNH_2$	$3.30x10^{-11}$	(2)
$CH_3 + N \rightarrow HCN + H + H$	$3.32x10^{-13}$	(2)
$N(\,_2D) + CH_3 \rightarrow H + CNH_2$	$1.00x10^{-10}$	(2)
$CH_4 + N \rightarrow CNH_4$	$3.01x10^{-18}$	(2)
$CH_4 + N \rightarrow HCN + H_2 + H$	$2.51x10^{-14}$	(2)
$N(\,_2D) + CH_4 \rightarrow CNH_3 + H$	$4.70x10^{-10} * e\left(-\frac{5820.0}{R_{gas} * T_{gas}}\right)$	(2)
$C_2H_3 + N \rightarrow C_2NH_2 + H$	0.80	(2)
$C_2H_3 + N \rightarrow C_2NH_3$	0.04	(2)
$C_2H_3 + N \rightarrow C_2H_2 + NH$	0.16	(2)
$C_2H_4 + N \rightarrow HCN + CH_3$	$4.20x10^{-14}$	(2)
$C_3H_6 + N \rightarrow C_2H_4 + HCN + H$	$2.49x10^{-13} * \left(\frac{T_{gas}}{298}\right)^{0.0} * e\left(-\frac{6900.0}{R_{gas} * T_{gas}}\right)$	(2)
$CH_4 + NH \rightarrow CH_3 + NH_2$	$1.49x10^{-10} * e\left(-\frac{83980.0}{R_{gas} * T_{gas}}\right)$	(2)
$C_2H_6 + NH \rightarrow C_2H_5 + NH_2$	$1.16x10^{-10} * e\left(-\frac{70010.0}{R_{gas} * T_{gas}}\right)$	(2)
$C + NH_2 \rightarrow CH + NH$	$9.61x10^{-13} * e\left(-\frac{87300.0}{R_{gas} * T_{gas}}\right)$	(2)

$CH_3 + NH_2 \rightarrow CNH_5$	$1.80x10^{-27} * \left(\frac{T_{gas}}{298}\right)^{-3.85}$	(2)
$CH_3 + NH_2 \rightarrow CH_4 + NH$	$8.40x10^{-17}$	(2)
$CH_4 + NH_2 \rightarrow CH_3 + NH_3$	$5.75x10^{-11} * e\left(-\frac{57800.0}{R_{gas} * T_{gas}}\right)$	(2)
$C_2H_2 + NH_2 \rightarrow C_2H + NH_3$	$1.34x10^{-12} * \left(\frac{T_{gas}}{298}\right)^{2.07} * e\left(-\frac{99770.0}{R_{gas} * T_{gas}}\right)$	(2)
$C_2H_4 + NH_2 \rightarrow C_2H_3 + NH_3$	$1.56x10^{-15} * \left(\frac{T_{gas}}{298}\right)^{4.80} * e\left(-\frac{29430.0}{R_{gas} * T_{gas}}\right)$	(2)
$C_2H_4 + NH_2 \rightarrow C_2NH_6$	$1.71x10^{-14} * \left(\frac{T_{gas}}{298}\right)^{2.98} * e\left(-\frac{11060.0}{R_{gas} * T_{gas}}\right)$	(2)
$C_2H_5 + NH_2 \rightarrow C_2H_6 + NH$	$1.18x10^{-14}$	(2)
$C_2H_6 + NH_2 \rightarrow C_2H_5 + NH_3$	$1.75x10^{-11} * e\left(-\frac{44000.0}{R_{gas} * T_{gas}}\right)$	(2)
$C_3H_6 + NH_2 \rightarrow C_3H_5 + NH_3$	$2.35x10^{-11} * e\left(-\frac{49600.0}{R_{gas} * T_{gas}}\right)$	(2)
$CH + NH_3 \rightarrow CNH_3 + H$	0.04	(2)
$CH_3 + NH_3 \rightarrow CH_4 + NH_2$	$4.95x10^{-14} * \left(\frac{T_{gas}}{298}\right)^{2.86} * e\left(-\frac{61030.0}{R_{gas} * T_{gas}}\right)$	(2)
$C_2H + NH_3 \rightarrow C_2H_2 + NH_2$	$1.73x10^{-13} * \left(\frac{T_{gas}}{298}\right)^{2.40} * e\left(\frac{6180.0}{R_{gas} * T_{gas}}\right)$	(2)
$C_2H_3 + NH_3 \rightarrow C_2H_4 + NH_2$	$3.36x10^{-16} * \left(\frac{T_{gas}}{298}\right)^{4.73} * e\left(-\frac{17630.0}{R_{gas} * T_{gas}}\right)$	(2)
$H + N_2H_3 \rightarrow NH_2 + NH_2$	$2.49x10^{-10} * e\left(-\frac{6280.0}{R_{gas} * T_{gas}}\right)$	(1)

$NH_2 + NH_2 \rightarrow H + N_2H_3$ (*)	$3.32x10^{-12} * \left(\frac{T_{gas}}{298}\right)^{0.51} * e\left(-\frac{211000.0}{R_{gas} * T_{gas}}\right)$	(2)
$C_2H_2 + N_2H_3 \rightarrow C_2NH_3 + NH_2$ (*)	$1.00x10^{-14} * e\left(-\frac{33260}{R_{gas} * T_{gas}}\right)$	(2)
$CNH_3 + N_2H_3 \rightarrow CNH_2 + N_2H_4$ (*)	$1.50x10^{-13} * \left(\frac{T_{gas}}{298}\right)^{2.70} * e\left(-\frac{48200}{R_{gas} * T_{gas}}\right)$	(2)
$N_2H_3 + H \rightarrow NH_3 + NH$ (*)	$6.55x10^{-12} * \left(\frac{T_{gas}}{298}\right)^{1.47} * e\left(-\frac{58100}{R_{gas} * T_{gas}}\right)$	(2)
$N_2H_3 + NH_3 \rightarrow NH_2 + N_2H_4$ (*)	$4.65x10^{-11} * e\left(-\frac{137000.0}{R_{gas} * T_{gas}}\right)$	(2)
$CNH_4 + N_2H_3 \rightarrow CN_2H_4 + NH_3$ (*)	$1.18x10^{-11} * \left(\frac{T_{gas}}{298}\right)^{0.12} * e\left(-\frac{1900}{R_{gas} * T_{gas}}\right)$	(2)
$CNH_4 + N_2H_3 \rightarrow CNH_3 + N_2H_4$ (*)	$5.16x10^{-12} * \left(\frac{T_{gas}}{298}\right)^{0.28} * e\left(\frac{3400}{R_{gas} * T_{gas}}\right)$	(2)
$CH_3 + N_2H_3 \rightarrow CNH_4 + NH_2$ (*)	$3.40x10^{-09} * \left(\frac{T_{gas}}{298}\right)^{-0.59} * e\left(-\frac{62840}{R_{gas} * T_{gas}}\right)$	(2)
$C_2H + N_2H_3 \rightarrow NH_2 + C_2NH_2$ (*)	$3.01x10^{-11}$	(2)
$C_2H_5 + N_2H_3 \rightarrow C_2NH_6 + NH_2$ (*)	$4.98x10^{-11}$	(2)
$C_2H_5 + N_2H_3 \rightarrow C_2H_4 + N_2H_4$ (*)	$2.97x10^{-12}$	(2)
$H_2 + N_2H_3 \rightarrow N_2H_4 + H$ (*)	$5.00x10^{-11} * e\left(-\frac{109000.0}{R_{gas} * T_{gas}}\right)$	(2)
$C_2NH_5 + N_2H_3 \rightarrow C_2NH_4 + N_2H_4$ (*)	$1.99x10^{-14} * e\left(-\frac{54210}{R_{gas} * T_{gas}}\right)$	(2)

$HCN + N_2H_3 \rightarrow CN + N_2H_4$ (*)	$1.47x10^{-13} * \left(\frac{T_{gas}}{298}\right)^{2.54} * e\left(-\frac{174000.0}{R_{gas} * T_{gas}}\right)$	(2)
$C_2H_6 + N_2H_3 \rightarrow C_2H_5 + N_2H_4$ (*)	$6.54x10^{-13} * \left(\frac{T_{gas}}{298}\right)^{2.69} * e\left(-\frac{79080}{R_{gas} * T_{gas}}\right)$	(2)
$CH_4 + N_2H_3 \rightarrow CH_3 + N_2H_4$ (*)	$4.21x10^{-14} * \left(\frac{T_{gas}}{298}\right)^{3.74} * e\left(-\frac{87910}{R_{gas} * T_{gas}}\right)$	(2)
$C_3H_6 + N_2H_3 \rightarrow C_3H_5 + N_2H_4$ (*)	$9.86x10^{-15} * \left(\frac{T_{gas}}{298}\right)^{4.40} * e\left(-\frac{56680}{R_{gas} * T_{gas}}\right)$	(2)
$CNH_5 + N_2H_3 \rightarrow CNH_4 + N_2H_4$ (*)	$8.66x10^{-16} * \left(\frac{T_{gas}}{298}\right)^{4.12} * e\left(-\frac{67930}{R_{gas} * T_{gas}}\right)$	(2)
$NH_3 + NH \rightarrow N_2H_3 + H$ (*)	$4.48x10^{-12} * \left(\frac{T_{gas}}{298}\right)^{0.97} * e\left(-\frac{287000}{R_{gas} * T_{gas}}\right)$	(2)
$C_2NH_4 + N_2H_4 \rightarrow C_2NH_5 + N_2H_3$ (*)	$3.01x10^{-13} * e\left(-\frac{34420}{R_{gas} * T_{gas}}\right)$	(2)
$C_2H_3 + N_2H_4 \rightarrow C_2H_4 + N_2H_3$ (*)	$2.01x10^{-14} * e\left(\frac{2490}{R_{gas} * T_{gas}}\right)$	(2)
$CNH_2 + N_2H_4 \rightarrow CNH_3 + N_2H_3$ (*)	$1.69x10^{-13} * e\left(-\frac{29020}{R_{gas} * T_{gas}}\right)$	(2)
$CNH_4 + NH_2 \rightarrow CH_3 + N_2H_3$ (*)	$4.14x10^{-21} * \left(\frac{T_{gas}}{298}\right)^{4.50} * e\left(-\frac{121000}{R_{gas} * T_{gas}}\right)$	(2)
$C_3H_5 + N_2H_4 \rightarrow C_3H_6 + N_2H_3$ (*)	$7.67x10^{-14} * \left(\frac{T_{gas}}{298}\right)^{2.05} * e\left(-\frac{56790}{R_{gas} * T_{gas}}\right)$	(2)
$CNH_3 + NH_3 \rightarrow CH_3 + N_2H_3$ (*)	$4.09x10^{-15} * \left(\frac{T_{gas}}{298}\right)^{2.68} * e\left(-\frac{429000}{R_{gas} * T_{gas}}\right)$	(2)
$C_3H_7 + N_2H_4 \rightarrow C_3H_8 + N_2H_3$ (*)	$5.15x10^{-15} * \left(\frac{T_{gas}}{298}\right)^{2.11} * e\left(-\frac{10730}{R_{gas} * T_{gas}}\right)$	(2)

$C_3H_8 + N_2H_3 \rightarrow C_3H_7 + N_2H_4$ (*)	$7.21x10^{-15} * \left(\frac{T_{gas}}{298}\right)^{4.12} * e\left(-\frac{63500}{R_{gas} * T_{gas}}\right)$	(2)
$CNH_4 + N_2H_4 \rightarrow CNH_5 + N_2H_3$ (*)	$5.00x10^{-15} * e\left(-\frac{10810}{R_{gas} * T_{gas}}\right)$	(2)
$N_2H_3 + H \rightarrow N_2H_4$ (*)	$2.32x10^{-19}$	(2)
$N_2H_4 \rightarrow H + N_2H_3$	$(4.5499x10^{15}) * (T_{gas})^{-7.69} * e\left(\frac{83700}{1.9872 * T_{gas}}\right)$	(2)
$N_2H_4 + H \rightarrow H_2 + N_2H_3$	$9.88x10^{-13} * \left(\frac{T_{gas}}{298}\right)^{2.56} * e\left(-\frac{5100}{R_{gas} * T_{gas}}\right)$	(2)
$N_2H_4 + CH_3 \rightarrow CH_4 + N_2H_3$	$1.04x10^{-14} * \left(\frac{T_{gas}}{298}\right)^{4.00} * e\left(-\frac{16940}{R_{gas} * T_{gas}}\right)$	(2)
$N_2H_4 + C_2H_5 \rightarrow C_2H_6 + N_2H_3$	$8.32x10^{-14} * e\left(-\frac{19210}{R_{gas} * T_{gas}}\right)$	(2)
$N_2H_4 \rightarrow NH_2 + NH_2$	$1.78x10^{-16} * e\left(-\frac{269000}{R_{gas} * T_{gas}}\right)$	(2)
$NH + N_2H_4 \rightarrow N_2H_3 + NH_2$	$8.65x10^{-14} * \left(\frac{T_{gas}}{298}\right)^{3.61} * e\left(-\frac{24300}{R_{gas} * T_{gas}}\right)$	(2)
$NH_2 + NH_2 \rightarrow N_2H_4$	$1.04x10^{-08} * \left(\frac{T_{gas}}{298}\right)^{-4.17} * e\left(-\frac{12930}{R_{gas} * T_{gas}}\right)$	(2)
$N_2H_4 + CH_2 \rightarrow CH_3 + N_2H_3$ (*)	$1.00x10^{-14}$	(2)
$N_2H_4 + H \rightarrow NH_2 + NH_3$ (*)	$1.69x10^{-11} * e\left(-\frac{14970}{R_{gas} * T_{gas}}\right)$	(2)
$HCN + N_2H_4 \rightarrow CN_2H_3 + NH_2$ (*)	$9.60x10^{-14} * \left(\frac{T_{gas}}{298}\right)^{2.09} * e\left(-\frac{22780}{R_{gas} * T_{gas}}\right)$	(2)

$CN_2H_3 + NH_2 \rightarrow HCN + N_2H_4$ (**)	$1.0 * e\left(\frac{-54.286306947830425}{R_{gas} * T_{gas}}\right)$	(6)
$CN + N \rightarrow C + N_2$	$1.07x10^{-13} * \left(\frac{T_{gas}}{298}\right)^{2.22} * e\left(-\frac{510000.0}{R_{gas} * T_{gas}}\right)$	(2)
$CN + N \rightarrow CN_2$	$2.76x10^{-32}$	(2)
$CN + NH_3 \rightarrow CN_2H_2 + H$	$0.05 * e\left(-\frac{70770.0}{R_{gas} * T_{gas}}\right)$	(2)
$CN + C \rightarrow C_2 + N$	$4.98x10^{-10} * e\left(-\frac{150000.0}{R_{gas} * T_{gas}}\right)$	(2)
$CN + CH_4 \rightarrow HCN + CH_3$	$5.11x10^{-13} * \left(\frac{T_{gas}}{298}\right)^{2.64} * e\left(\frac{1250.0}{R_{gas} * T_{gas}}\right)$	(2)
$CN + C_2H_2 \rightarrow HCN + C_2H$	$2.19x10^{-10}$	(2)
$CN + C_2H_4 \rightarrow HCN + C_2H_3$	$2.09x10^{-10}$	(2)
$CN + C_2H_6 \rightarrow HCN + C_2H_5$	$3.50x10^{-12} * \left(\frac{T_{gas}}{298}\right)^{2.16} * e\left(-\frac{5190.0}{R_{gas} * T_{gas}}\right)$	(2)
$CN + CN \rightarrow N_2 + C_2$	$1.66x10^{-11}$	(2)
$CN \rightarrow C + N$	$1.00x10^{-09} * e\left(-\frac{590000.0}{R_{gas} * T_{gas}}\right)$	(2)
$CN + CNH_5 \rightarrow CN_2H_2 + CH_3$	$3.72x10^{-12} * \left(\frac{T_{gas}}{298}\right)^{-1.80} * e\left(-\frac{60.0}{R_{gas} * T_{gas}}\right)$	(2)
$C_2N + N \rightarrow CN + CN$	$1.00x10^{-10} * \left(\frac{T_{gas}}{298}\right)^{-0.00}$	(2)
$CN_2 + CN_2 \rightarrow CN + CN + N_2$	$6.14x10^{-12}$	(2)

$C_2N2 + H \rightarrow CN + HCN$	$5.25x10^{-10} * \left(\frac{T_{gas}}{298}\right)^{-0.00} * e\left(-\frac{33510.0}{R_{gas} * T_{gas}}\right)$	(2)
$C_2N2 + C \rightarrow CN + C_2N$	$3.01x10^{-11}$	(2)
$C_2N2 \rightarrow CN + CN$	$2.97x10^{-07} * \left(\frac{T_{gas}}{298}\right)^{-0.00} * e\left(-\frac{446000.0}{R_{gas} * T_{gas}}\right)$	(2)
$C_2NH_3 + H \rightarrow CN + CH_4$	$1.66x10^{-13} * \left(\frac{T_{gas}}{298}\right)^{-0.00} * e\left(-\frac{12470.0}{R_{gas} * T_{gas}}\right)$	(2)
$HCN + H \rightarrow CN + H_2$	$1.95x10^{-10} * \left(\frac{T_{gas}}{298}\right)^{1.92} * e\left(-\frac{110000.0}{R_{gas} * T_{gas}}\right)$	(2)
$HCN \rightarrow CN + H$	$1.93x10^{-04} * \left(\frac{T_{gas}}{298}\right)^{-2.44} * e\left(-\frac{522000.0}{R_{gas} * T_{gas}}\right)$	(2)
$CH + N2 \rightarrow CN2 + H$	$7.82x10^{-13} * \left(\frac{T_{gas}}{298}\right)^{0.53} * e\left(-\frac{71200.0}{R_{gas} * T_{gas}}\right)$	(2)
$HCN + C2 \rightarrow H + C_3N$	$1.12x10^{-10} * \left(\frac{T_{gas}}{298}\right)^{-0.82} * e\left(-\frac{80.0}{R_{gas} * T_{gas}}\right)$	(2)
$HCN \rightarrow HCN$	$1.70x10^{13} * \left(\frac{T_{gas}}{298}\right)^{0.92} * e\left(-\frac{178000.0}{R_{gas} * T_{gas}}\right)$	(2)
$CN + HCN \rightarrow C_2N_2 + H$	$5.90x10^{-11} * \left(\frac{T_{gas}}{298}\right)^{1.74} * e\left(-\frac{56480.0}{R_{gas} * T_{gas}}\right)$	(2)
$CN + CN \rightarrow C_2N_2$	$4.94x10^{-29} * \left(\frac{T_{gas}}{298}\right)^{-2.62}$	(2)
$CNH_3 + NH \rightarrow NH_2 + CNH_2$	$5.88x10^{-15} * \left(\frac{T_{gas}}{298}\right)^{3.92} * e\left(-\frac{6520.0}{R_{gas} * T_{gas}}\right)$	(2)
$CNH_3 + H \rightarrow H_2 + CNH_2$	$8320 * e\left(-\frac{10000.0}{R_{gas} * T_{gas}}\right)$	(2)
$CNH_2 + N \rightarrow NH + HCN$	$1.20x10^{-11} * e\left(-\frac{6300.0}{R_{gas} * T_{gas}}\right)$	(2)

$CNH_2 + CNH_2 \rightarrow HCN + CNH_3$	$3.70x10^{-14}$	(2)
$CNH_2 \rightarrow HCN + H$	$7.90x10^{13} * e\left(-\frac{141000.0}{R_{gas} * T_{gas}}\right)$	(2)
$C_2NH_3 + N \rightarrow HCN + HCN + H$	$2.27x10^{-15} * e\left(-\frac{6760.0}{R_{gas} * T_{gas}}\right)$	(2)
$C_2NH_3 + CH_3 \rightarrow CH_4 + C_2NH_2$	$1.66x10^{-14}$	(2)
$H + C_2NH_3 \rightarrow C_2NH_4$	$1.11x10^{-11} * \left(\frac{T_{gas}}{298}\right)^{1.49} * e\left(-\frac{27600.0}{R_{gas} * T_{gas}}\right)$	(2)
$CN_2H_2 + H \rightarrow CH_3 + N_2$	$1.60x10^{-11}$	(2)
$CN_2H_2 + NH_2 \rightarrow NH_3 + CN_2H$	$1.41x10^{-11} * \left(\frac{T_{gas}}{298}\right)^{-0.00} * e\left(-\frac{27270.0}{R_{gas} * T_{gas}}\right)$	(2)
$CN_2H_2 \rightarrow N_2 + CH_2$	$1.20x10^{12} * \left(\frac{T_{gas}}{298}\right)^{-0.00} * e\left(-\frac{142000.0}{R_{gas} * T_{gas}}\right)$	(2)
$H + C_2NH_5 \rightarrow C_2NH_6$	$1.22x10^{-11} * \left(\frac{T_{gas}}{298}\right)^{1.51} * e\left(-\frac{7680.0}{R_{gas} * T_{gas}}\right)$	(2)
$H + CNH_2 \rightarrow HCN + H_2$	$1.80x10^{-11}$	(2)
$CN2 + H \rightarrow HCN + N$	$2.87x10^{-16} * \left(\frac{T_{gas}}{298}\right)^{4.69} * e\left(-\frac{10180.0}{R_{gas} * T_{gas}}\right)$	(2)
$CH_3 + N \rightarrow HCN + H_2$	0.10	(2)
$C_2NH_3 + H \rightarrow HCN + CH_3$	$3.39x10^{-12} * e\left(-\frac{32840.0}{R_{gas} * T_{gas}}\right)$	(2)

$HCN + H \rightarrow HCN + H$	$1.13x10^{-13}$	(2)
$CN + H \rightarrow HCN$	$9.35x10^{-30} * \left(\frac{T_{gas}}{298}\right)^{-2.00} * e\left(-\frac{43300.0}{R_{gas} * T_{gas}}\right)$	(2)
$CN + NH_3 \rightarrow HCN + NH_2$	$2.91x10^{-11}$	(2)
$CN + H_2 \rightarrow HCN + H$	$1.31x10^{-13} * \left(\frac{T_{gas}}{298}\right)^{1.57} * e\left(-\frac{44730.0}{R_{gas} * T_{gas}}\right)$	(2)
$CNH_3 + NH_2 \rightarrow CNH_2 + NH_3$ (*)	$2.18x10^{-12} * \left(\frac{T_{gas}}{298}\right)^{1.74} * e\left(\frac{1.05}{R_{gas} * T_{gas}}\right)$	(2)
$CNH_2 + NH_3 \rightarrow CNH_3 + NH_2$ (*)	$8.54x10^{-13} * \left(\frac{T_{gas}}{298}\right)^{1.35} * e\left(-\frac{109000}{R_{gas} * T_{gas}}\right)$	(2)
$CNH_3 + C_2H_3 \rightarrow C_2H_4 + CNH_2$ (*)	$3.21x10^{-15} * \left(\frac{T_{gas}}{298}\right)^{4.21} * e\left(-\frac{6790}{R_{gas} * T_{gas}}\right)$	(2)
$CNH_3 + CH_3 \rightarrow CH_4 + CNH_2$ (*)	$2.04x10^{-15} * \left(\frac{T_{gas}}{298}\right)^{3.92} * e\left(-\frac{19330}{R_{gas} * T_{gas}}\right)$	(2)
$CNH_3 + C_2H_5 \rightarrow C_2H_6 + CNH_2$ (*)	$8.19x10^{-14} * \left(\frac{T_{gas}}{298}\right)^{2.81} * e\left(-\frac{24530}{R_{gas} * T_{gas}}\right)$	(2)
$CH_4 + CNH_2 \rightarrow CNH_3 + CH_3$ (*)	$2.39x10^{-15} * \left(\frac{T_{gas}}{298}\right)^{3.87} * e\left(-\frac{89330}{R_{gas} * T_{gas}}\right)$	(2)
$CNH_3 + CN \rightarrow HCN + CNH_2$ (*)	$1.51x10^{-14} * \left(\frac{T_{gas}}{298}\right)^{2.72} * e\left(\frac{5970}{R_{gas} * T_{gas}}\right)$	(2)
$CNH_2 + H \rightarrow CNH_3$ (*)	$3.21x10^{-30} * \left(\frac{T_{gas}}{298}\right)^{-2.57} * e\left(-\frac{1790}{R_{gas} * T_{gas}}\right)$	(2)
$CNH_2 + NH_2 \rightarrow HCN + NH_3$ (*)	$8.30x10^{-11}$	(2)
$CH_3 + CNH_2 \rightarrow CH_4 + HCN$	$4.40x10^{-11}$	(2)

(*)		
$C_2H_6 + CNH_2 \rightarrow CNH_3 + C_2H_5$ (*)	$6.71x10^{-15} * \left(\frac{T_{gas}}{298}\right)^{3.74} * e\left(-\frac{70850}{R_{gas} * T_{gas}}\right)$	(2)
$HCN + NH_2 \rightarrow CN_2H_3$ (*)	$6.44x10^{-16} * \left(\frac{T_{gas}}{298}\right)^{-2.68} * e\left(-\frac{3600.0}{R_{gas} * T_{gas}}\right)$	(2)
$CN_2H_3 \rightarrow HCN + NH_2$ (*)	$4.92x10^{-29} * \left(\frac{T_{gas}}{298}\right)^{-2.40} * e\left(-\frac{157000.0}{R_{gas} * T_{gas}}\right)$	(2)
$CN_2H_3 + C_2H_2 \rightarrow CN_2H_2 + C_2H_3$ (*)	$3.01x10^{-14}$	(2)
$CN_2H_3 + C_2H_4 \rightarrow CN_2H_2 + C_2H_5$ (*)	$1.00x10^{-14}$	(2)
$CN_2H_3 + NH \rightarrow CN_2H_2 + NH_2$ (*)	$1.44x10^{-11}$	(2)
$CN_2H_3 + NH_2 \rightarrow CN_2H_2 + NH_3$ (*)	$1.03x10^{-11}$	(2)
$CN_2H_3 + CH_3 \rightarrow C_2NH_3 + NH_3$ (*)	$5.81x10^{-11} * \left(\frac{T_{gas}}{298}\right)^{0.10}$	(2)
$C_2NH_3 \rightarrow C_2NH_2 + H$ (*)	$1.00x10^{-16} * \left(\frac{T_{gas}}{298}\right)^{-0.00} * e\left(-\frac{402000.0}{R_{gas} * T_{gas}}\right)$	(2)
$CN_2H_4 \rightarrow HCN + NH_3$ (*)	$2.82x10^{-7} * \left(\frac{T_{gas}}{298}\right)^{8.36} * e\left(-\frac{245000.0}{R_{gas} * T_{gas}}\right)$	(2)
$HCN + NH_3 \rightarrow CN_2H_4$ (*)	$5.11x10^{-15} * \left(\frac{T_{gas}}{298}\right)^{3.10} * e\left(-\frac{243000.0}{R_{gas} * T_{gas}}\right)$	(2)
$CNH_2 + NH_2 \rightarrow CN_2H_4$ (*)	$6.10x10^{-12} * \left(\frac{T_{gas}}{298}\right)^{1.48} * e\left(-\frac{4690.0}{R_{gas} * T_{gas}}\right)$	(2)

$C_2NH_6 + NH \rightarrow CN_2H_4 + CH_3$ (*)	$3.90x10^{-10} * \left(\frac{T_{gas}}{298}\right)^{0.18} * e\left(-\frac{4.07}{R_{gas} * T_{gas}}\right)$	(2)
$CNH_3 + NH_2 \rightarrow CN_2H_4 + H$ (*)	$2.01x10^{-13}$	(2)
$CN_2H_4 + NH_2 \rightarrow CN_2H_3 + NH_3$ (*)	$9.85x10^{-13} * e\left(-\frac{8610}{R_{gas} * T_{gas}}\right)$	(2)
$CN_2H_4 \rightarrow H_2 + CN_2H_2$ (*)	$4.46x10^{-13} * e\left(-\frac{286000}{R_{gas} * T_{gas}}\right)$	(2)
$H_2 + C_2NH_2 \rightarrow C_2NH_3 + H$ *assumed the same rate coefficient of H_2+C_2NH_4*	$2.18x10^{-13} * \left(\frac{T_{gas}}{298}\right)^{1.82} * e\left(-\frac{73670.0}{R_{gas} * T_{gas}}\right)$	(2)
$C_2H_3 + NH_2 \rightarrow C_2NH_3 + H_2$ (*)	$2.22x10^{-12} * \left(\frac{T_{gas}}{298}\right)^{-1.52} * e\left(-\frac{3020.0}{R_{gas} * T_{gas}}\right)$	(2)
$C_2NH_4 \rightarrow C_2NH_3 + H$ (*)	$4.63x10^{12} * \left(\frac{T_{gas}}{298}\right)^{1.62} * e\left(-\frac{94780.0}{R_{gas} * T_{gas}}\right)$	(2)
$C_2NH_4 + CH_2 \rightarrow C_2NH_3 + CH_3$ (*)	$3.01x10^{-11}$	(2)
$NH_2 + C_2NH_2 \rightarrow C_2NH_3 + NH$ (*)	$1.76x10^{-13} * \left(\frac{T_{gas}}{298}\right)^{1.99} * e\left(-\frac{47200.0}{R_{gas} * T_{gas}}\right)$	(2)
$CH_3 + C_2NH_4 \rightarrow CH_4 + C_2NH_3$ (*)	$1.01x10^{-11}$	(2)
$HCN + CH_2 \rightarrow C_2NH_3$ (*)	$1.00x10^{-15}$	(2)
$C_2H_2 + NH_2 \rightarrow H + C_2NH_3$ (*)	$4.12x10^{-13} * \left(\frac{T_{gas}}{298}\right)^{2.30} * e\left(-\frac{56460.0}{R_{gas} * T_{gas}}\right)$	(2)
$C_2H_4 + NH \rightarrow C_2NH_3 + H_2$ (*)	$5.50x10^{-12} * \left(\frac{T_{gas}}{298}\right)^{-1.83} * e\left(-\frac{13300.0}{R_{gas} * T_{gas}}\right)$	(2)

$C_2NH_4 + C_2NH_4 \rightarrow C_2NH_5 + C_2NH_3$ (*)	$1.49x10^{-11}$	(2)
$C_2NH_3 + CH_2 \rightarrow C_2H_4 + HCN$ (*)	$1.59x10^{-12} * \left(\frac{T_{gas}}{298}\right)^{1.49} * e\left(-\frac{33160.0}{R_{gas} * T_{gas}}\right)$	(2)
$C_2NH_3 + CH_3 \rightarrow HCN + C_2H_5$ (*)	$2.71x10^{-13} * \left(\frac{T_{gas}}{298}\right)^{2.34} * e\left(-\frac{44900.0}{R_{gas} * T_{gas}}\right)$	(2)
$CH_4 + C_2NH_2 \rightarrow C_2NH_3 + CH_3$ *assumed the same rate coefficient of CH_4+C_2NH_4*	$4.82x10^{-14} * \left(\frac{T_{gas}}{298}\right)^{2.88} * e\left(-\frac{89800.0}{R_{gas} * T_{gas}}\right)$	(2)
$HCN + CH_3 \rightarrow C_2NH_4$ (*)	$2.99x10^{-13} * e\left(-\frac{25400.0}{R_{gas} * T_{gas}}\right)$	(2)
$C_2NH_5 + CH_3 \rightarrow CH_4 + C_2NH_4$ (*)	$2.66x10^{-12} * e\left(-\frac{33470.0}{R_{gas} * T_{gas}}\right)$	(2)
$C_2NH_5 + C_2H_5 \rightarrow C_2H_6 + C_2NH_4$ (*)	$2.09x10^{-12} * e\left(-\frac{35590.0}{R_{gas} * T_{gas}}\right)$	(2)
$C_2NH_4 \rightarrow HCN + CH_3$ (*)	$2.94x10^{14} * \left(\frac{T_{gas}}{298}\right)^{-5.76} * e\left(-\frac{81500.0}{R_{gas} * T_{gas}}\right)$	(2)
$C_2H_6 + C_2NH_4 \rightarrow C_2H_5 + C_2NH_5$ (*)	$1.91x10^{-13} * \left(\frac{T_{gas}}{298}\right)^{2.75} * e\left(-\frac{73330.0}{R_{gas} * T_{gas}}\right)$	(2)
$CH_4 + C_2NH_4 \rightarrow C_2NH_5 + CH_3$ (*)	$4.82x10^{-14} * \left(\frac{T_{gas}}{298}\right)^{2.88} * e\left(-\frac{89800.0}{R_{gas} * T_{gas}}\right)$	(2)
$C_2H_3 + NH_2 \rightarrow C_2NH_5$ (*)	$8.25x10^{-11} * \left(\frac{T_{gas}}{298}\right)^{-0.61} * e\left(\frac{320.0}{R_{gas} * T_{gas}}\right)$	(2)
$CNH_2 + C_2NH_4 \rightarrow C_2NH_5 + HCN$ (*)	$1.50x10^{-11}$	(2)

$CH_3 + CNH_2 \rightarrow C_2NH_5$ (*)	$4.65x10^{-11}$	(2)
$C_2NH_6 \rightarrow C_2NH_5 + H$ (*)	$1.25x10^{14} * \left(\frac{T_{gas}}{298}\right)^{-2.15} * e\left(-\frac{92030.0}{R_{gas} * T_{gas}}\right)$	(2)
$C_2NH_6 + H \rightarrow C_2H_4 + NH_3$ (*)	$2.63x10^{-10} * \left(\frac{T_{gas}}{298}\right)^{-3.02} * e\left(-\frac{11910.0}{R_{gas} * T_{gas}}\right)$	(2)
$C_2NH_6 + H \rightarrow CNH_3 + CH_4$ (*)	$8.73x10^{-17} * \left(\frac{T_{gas}}{298}\right)^{2.10} * e\left(-\frac{890000.0}{R_{gas} * T_{gas}}\right)$	(2)
$CH_3^+ + NH_3 \rightarrow NH_4^+ + CH_2$	$3.04x10^{-10} * \left(\frac{T_{gas}}{300}\right)^{-0.50}$	(3)
$CH_4^+ + NH_3 \rightarrow NH_4^+ + CH_3$	$1.15x10^{-9} * \left(\frac{T_{gas}}{300}\right)^{-0.50}$	(3)
$H_3^+ + NH_3 \rightarrow NH_4^+ + H_2$	$4.39x10^{-9} * \left(\frac{T_{gas}}{300}\right)^{-0.50}$	(3)
$NH_3 + CH_5^+ \rightarrow NH_4^+ + CH_4$	$2.50x10^{-9} * \left(\frac{T_{gas}}{300}\right)^{-0.50}$	(3)
$CH_4^+ + NH_3 \rightarrow NH_3^+ + CH_4$	$1.65x10^{-9} * \left(\frac{T_{gas}}{300}\right)^{-0.50}$	(3)
$NH_3 + HCN^+ \rightarrow HCN + NH_3^+$	$1.68x10^{-9} * \left(\frac{T_{gas}}{300}\right)^{-0.50}$	(3)
$H^{3+} + NH_2 \rightarrow NH_3^+ + H_2$	$1.80x10^{-9} * \left(\frac{T_{gas}}{300}\right)^{-0.50}$	(3)
$NH_2 + CH_5^+ \rightarrow NH_3^+ + CH_4$	$9.90x10^{-10} * \left(\frac{T_{gas}}{300}\right)^{-0.50}$	(3)
$NH_2 + HCN^+ \rightarrow CN + NH_3^+$	$9.00x10^{-10} * \left(\frac{T_{gas}}{300}\right)^{-0.50}$	(3)

$H_2 + NH_3^+ \rightarrow NH_2 + CH_3^+$	$9.60x10^{-10}$	(3)
$CH_4 + NH_3^+ \rightarrow NH_4^+ + CH_3$	$4.80x10^{-10}$	(3)
$CH + NH_3^+ \rightarrow NH_4^+ + C$	$6.90x10^{-10} * \left(\frac{T_{gas}}{300}\right)^{-0.50}$	(3)
$H_2 + NH_3^+ \rightarrow NH_4^+ + H$	$3.09x10^{-13} * \left(\frac{T_{gas}}{300}\right)^{-1.08} * e\left(\frac{50.90}{T_{gas}}\right)$	(3)
$NH_2 + NH_3^+ \rightarrow NH_4^+ + NH$	$1.00x10^{-11} * \left(\frac{T_{gas}}{300}\right)^{-0.50}$	(3)
$NH + NH_3^+ \rightarrow NH_4^+ + N$	$7.10x10^{-10} * \left(\frac{T_{gas}}{300}\right)^{-0.50}$	(3)
$NH^+ + H_2 \rightarrow NH_2^+ + H$	$0.85 * 1.23x10^{-9}$	(3)
$NH_2^+ + H_2 \rightarrow NH_3^+ + H$	$1.95x10^{-10}$	(3)
$H^+ + NH_2 \rightarrow NH_2^+ + H$	$2.90x10^{-9} * \left(\frac{T_{gas}}{300}\right)^{-0.50}$	(3)
$H_2^+ + NH_2 \rightarrow NH_2^+ + H_2$	$2.10x10^{-9} * \left(\frac{T_{gas}}{300}\right)^{-0.50}$	(3)
$N^+ + NH_2 \rightarrow NH_2^+ + N$	$1.00x10^{-9} * \left(\frac{T_{gas}}{300}\right)^{-0.50}$	(3)
$H^+ + CNH_3 \rightarrow NH_2^+ + CH_2$	$1.00x10^{-9} * \left(\frac{T_{gas}}{300}\right)^{-0.50}$	(3)
$H_2^+ + NH \rightarrow NH_2^+ + H$	$7.60x10^{-10} * \left(\frac{T_{gas}}{300}\right)^{-0.50}$	(3)
$H_2^+ + NH \rightarrow NH_2^+ + H_2$	$1.30x10^{-9} * \left(\frac{T_{gas}}{300}\right)^{-0.50}$	(3)
$CH_2 + NH_2^+ \rightarrow CH_3^+ + NH$	$4.90x10^{-10} * \left(\frac{T_{gas}}{300}\right)^{-0.00}$	(3)

$NH_2^+ + NH_2 \rightarrow NH_3^+ + NH$	$1.00x10^{-9} * \left(\frac{T_{gas}}{300}\right)^{-0.50}$	(3)
$NH + NH_2^+ \rightarrow NH_3^+ + N$	$7.30x10^{-10} * \left(\frac{T_{gas}}{300}\right)^{-0.50}$	(3)
$N^+ + H_2 \rightarrow NH^+ + H$	$5.0x10^{-10}$	(3)
$NH^+ + H_2 \rightarrow H_3^+ + N$	$0.15 * 1.23x10^{-9}$	(3)
$H^+ + NH \rightarrow NH^+ + H$	$2.10x10^{-9} * \left(\frac{T_{gas}}{300}\right)^{-0.50}$	(3)
$H_2^+ + NH \rightarrow NH^+ + H_2$	$7.60x10^{-10} * \left(\frac{T_{gas}}{300}\right)^{-0.50}$	(3)
$N^+ + NH \rightarrow NH^+ + N$	$3.70x10^{-10} * \left(\frac{T_{gas}}{300}\right)^{-0.50}$	(3)
$H_2^+ + N \rightarrow NH^+ + H$	$1.90x10^{-9}$	(3)
$CH_2 + NH^+ \rightarrow CH_3^+ + N$	$1.40x10^{-9}$	(3)
$NH^+ + C_2 \rightarrow HCN^+ + C$	$4.90x10^{-10}$	(3)
$NH^+ + CN \rightarrow HCN^+ + N$	$1.60x10^{-9} * \left(\frac{T_{gas}}{300}\right)^{-0.50}$	(3)
$NH^+ + NH_2 \rightarrow NH_3^+ + N$	$1.50x10^{-9}$	(3)
$NH^+ + NH \rightarrow NH_2^+ + N$	$1.00x10^{-9} * \left(\frac{T_{gas}}{300}\right)^{-0.50}$	(3)
$N^+ + CH_4 \rightarrow CH_4^+ + N$	$2.80x10^{-11}$	(3)
$N^+ + HCN \rightarrow HCN^+ + N$	$3.70x10^{-9} * \left(\frac{T_{gas}}{300}\right)^{-0.50}$	(3)

$N^+ + CH_4 \rightarrow CH_3^+ + N + H$	$4.70x10^{-10}$	(3)
$N^+ + CH_4 \rightarrow HCN^+ + H_2 + H$	$5.60x10^{-11}$	(3)
$H_2^+ + CN \rightarrow HCN^+ + H$	$1.20x10^{-9} * \left(\frac{T_{gas}}{300}\right)^{-0.50}$	(3)
$H_3^+ + CN \rightarrow HCN^+ + H_2$	$2.00x10^{-9} * \left(\frac{T_{gas}}{300}\right)^{-0.50}$	(3)
$H + HCN^+ \rightarrow HCN + H^+$	$3.70x10^{-11}$	(3)
$CH_2 + HCN^+ \rightarrow CN + CH_3^+$	$8.70x10^{-10}$	(3)
$NH + HCN^+ \rightarrow CN + NH_2^+$	$6.50x10^{-10} * \left(\frac{T_{gas}}{300}\right)^{-0.50}$	(3)
$N^+ + NH_3 \rightarrow NH_2^+ + NH$	$0.20 * 2.35x10^{-9}$	(3)
$N^+ + NH_3 \rightarrow NH_3^+ + N$	$0.71 * 2.35x10^{-9}$	(3)
$H_2^+ + NH_3 \rightarrow NH_3^+ + H_2$	$5.70x10^{-9}$	(3)
$H^+ + NH_3 \rightarrow NH_3^+ + H$	$5.20x10^{-9}$	(3)
$NH^+ + NH_3 \rightarrow NH_3^+ + NH$	$0.75 * 2.40x10^{-9}$	(3)
$NH^+ + NH_3 \rightarrow NH_4^+ + N$	$0.25 * 2.40x10^{-9}$	(3)
$NH_2^+ + NH_3 \rightarrow NH_3^+ + NH_2$	$0.5 * 2.30x10^{-9}$	(3)
$NH_2^+ + NH_3 \rightarrow NH_4^+ + NH$	$0.5 * 2.30x10^{-9}$	(3)
$NH_3^+ + NH_3 \rightarrow NH_4^+ + NH_2$	$2.10x10^{-9}$	(3)

$H_2 + H_2^+ \rightarrow H + H_3^+$	$2.11x10^{-9}$	(3)
$H_2 + H_2 + H^+ \rightarrow H_2 + H_3^+$	$3.1x10^{-29} * \left(\frac{300.0}{T_{gas}}\right)^{0.5}$	(3)
$H_2^+ + H_2 \rightarrow H_2 + H^+ + H$	$1.00x10^{-08} * e\left(-\frac{84100.0}{T_{gas}}\right)$	(3)
$H_2^+ + H \rightarrow H_3^+$	$2.10x10^{-09}$	(3)
$H_2^+ + H \rightarrow H_2 + H^+$	$6.39x10^{-10}$	(3)
$H^+ + H_2 + M \rightarrow H_3^+ + M$	$1.50x10^{-29}$	(3)
$H^+ + H + M \rightarrow H_2^+ + M$	$1.00x10^{-34}$	(3)
$CH_5^+ + CH_2 \rightarrow CH_3^+ + CH_4$	$0.960x10^{-9}$	(3)
$CH_5^+ + H \rightarrow CH_4^+ + H_2$	$0.150x10^{-9}$	(3)
$CH_4^+ + CH_4 \rightarrow CH_5^+ + CH_3$	$0.150x10^{-8}$	(3)
$CH_4^+ + H_2 \rightarrow CH_5^+ + H$	$4.89x10^{-11} * \left(\frac{300.0}{T_{gas}}\right)^{0.14} * e\left(-\frac{36.10}{T_{gas}}\right)$	(3)
$CH_4^+ + H \rightarrow CH_3^+ + H_2$	$0.100x10^{-10}$	(3)
$CH_3^+ + CH_4 \rightarrow CH_4^+ + CH_3$	$0.136x10^{-9}$	(3)
$CH_3^+ + H_2 \rightarrow CH_4^+ + H$	$1.58x10^{-9}$	(3)
$H_3^+ + CH_4 \rightarrow CH_5^+ + H_2$	$2.40x10^{-9}$	(3)
$H_3^+ + CH_3 \rightarrow CH_4^+ + H_2$	$2.10x10^{-9}$	(3)

$H_3^+ + CH_2 \rightarrow CH_3^+ + H_2$	$1.70x10^{-9}$	(3)
$H_2^+ + CH_4 \rightarrow CH_5^+ + H$	$1.14x10^{-10}$	(3)
$H_2^+ + CH_4 \rightarrow CH_4^+ + H_2$	$1.40x10^{-9}$	(3)
$H_2^+ + CH_4 \rightarrow CH_3^+ + H_2 + H$	$2.30x10^{-9}$	(3)
$H_2^+ + CH_2 \rightarrow CH_3^+ + H$	$1.00x10^{-9}$	(3)
$H^+ + CH_4 \rightarrow CH_4^+ + H$	$1.50x10^{-9}$	(3)
$H^+ + CH_4 \rightarrow CH_3^+ + H_2$	$2.30x10^{-9}$	(3)
$H^+ + CH_3 \rightarrow CH_3^+ + H$	$3.40x10^{-9}$	(3)
$CN + H + M \rightarrow HCN + M$	$8.63x10^{-30} * \left(\frac{T_{gas}}{298.0}\right)^{-2.20} * e\left(-\frac{4.71}{8.314472x10^{-3} * T_{gas}}\right)$	(2)
$CN_2 + M \rightarrow C + N_2 + M$	$1.48x10^{-9} * e\left(-\frac{260.0}{8.314472x10^{-3} * T_{gas}}\right)$	(2)
$N + CN + M \rightarrow CN_2 + M$	$2.76x10^{-32}$	(2)
$N + CN_2 \rightarrow N_2 + CN$	$\left(\frac{1.0x10^{13}}{6.0223x10^{23}}\right)$	(2)
$CN_2 + M \rightarrow N + CN + M$	$\left(\frac{5.1x10^{15}}{6.0223x10^{23}}\right) * e\left(-\frac{53300.0}{TGAS}\right)$	(2)
$C + CN_2 \rightarrow CN + CN$	$\left(\frac{1.0x10^{13}}{6.0223x10^{23}}\right)$	(2)
$N + H + M \rightarrow NH + M$	$5.02x10^{-32}$	(2)

$N + H_2 + M \rightarrow NH_2 + M$	$1.00x10^{-26}$	(1)
$NH_2 + NH \rightarrow N_2H_3$	$1.16x10^{-10}$	(1)
$NH_2 + N_2H_4 \rightarrow NH_3 + N_2H_3$	$6.46x10^{-15} * \left(\frac{T_{gas}}{298.0}\right)^{3.60} * e\left(-\frac{3.21}{8.314472x10^{-3} * T_{gas}}\right)$	(1)
$M + NH_2 + H \rightarrow NH_3 + M$	$K_{\inf} = (7.6x10^{-35}) * T_{gas}^{0.387} * e\left(\frac{7840}{T_{gas}}\right)$ $K_0 = (7.6x10^{-10}) * e\left(-\frac{850}{T_{gas}}\right)$ $F = (0.58) * e\left(-\frac{T_{gas}}{4581}\right) + 0.42 * e\left(-\frac{T_{gas}}{102}\right)$	(8)
$M + NH_3 \rightarrow NH_2 + H + M$	$K_{\inf} = (3.1x10^{-8}) * e\left(-\frac{46860}{T_{gas}}\right)$ $K_0 = (2.8x10^{17}) * T_{gas}^{-0.39} * e\left(-\frac{55525}{T_{gas}}\right)$ $F = (0.58) * e\left(-\frac{T_{gas}}{4581}\right) + 0.42 * e\left(-\frac{T_{gas}}{102}\right)$	(8)
$CH_3 + CH_3 \rightarrow C_2H_6$	$1.62x10^{10} * \left(\frac{T_{gas}}{298.15}\right)^{-1.20} * e\left(-\frac{2450.0}{R_{gas} * T_{gas}}\right)$	(5)
$CH_3 + C_2H_5 \rightarrow C_3H_8$	$5.16x10^{-11} * \left(T_{gas}^{-0.32}\right)$	(5)
$C_2H_6 \rightarrow CH_3 + CH_3$	$4.62x10^{8} * \left(\frac{T_{gas}}{298.15}\right)^{-1.57} * e\left(-\frac{372000.0}{R_{gas} * T_{gas}}\right)$	(5)
$H + C_2H_4 \rightarrow C_2H_5$	$1.25x10^{-11} * \left(\frac{T_{gas}}{298}\right)^{1.07} * e\left(-\frac{6070.0}{R_{gas} * T_{gas}}\right)$	(5)
$C_2H_4 \rightarrow C_2H_2 + H_2$	$2.57x10^{8} * e\left(-\frac{167000.0}{R_{gas} * T_{gas}}\right)$	(5)

$CH_2 + H \rightarrow CH_3$	$K_{\inf} = \left(\frac{1.0}{0.64}\right) * (9.00x10^{-32}) * e\left(-\frac{550.0}{T_{gas}}\right)$ $K_0 = (8.55x10^{-12}) * T_{gas}^{0.15}$ $F = (1 - 0.562) * e\left(-\frac{T_{gas}}{91.0}\right) + 0.562 * e\left(-\frac{T_{gas}}{5836}\right) + e\left(-\frac{8552}{T_{gas}}\right)$	(5)
$CH + H_2 \rightarrow CH_3$	$K_{\inf} = \left(\frac{1.0}{0.64}\right) * (4.70x10^{-26}) * T_{gas}^{-1.60}$ $K_0 = (8.50x10^{-11}) * T_{gas}^{0.15}$ $F = (1 - 0.578) + \left(0.25 * e\left(-\frac{T_{gas}}{300.0}\right)\right)$	(5)
$H + C_2H_5 \rightarrow C_2H_6$	$K_{inf} = \left(\frac{0.56}{1.0}\right) * (4.00x10^{-19}) * T_{gas}^{-3.00} * e\left(-\frac{600.0}{T_{gas}}\right)$ $K_0 = (2.25x10\text{^}(-10)) * ((T\_gas/298)\text{^}0.16)$ $F = (1 - 0.842) * e\left(-\frac{T_{gas}}{125.0}\right) + 0.842 * e\left(-\frac{T_{gas}}{2219}\right) + e\left(-\frac{6682}{T_{gas}}\right)$	(5)
$H + C_2H_3 \rightarrow C_2H_4$	$K_{\inf} = (3.50x10^{-27})$ $K_0 = (2.02x10^{-10}) * \left(\left(\frac{T_{gas}}{298}\right)^{0.20}\right)$ $F = 0.5$	(5)
$H + C_2H_2 \rightarrow C_2H_3$	$K_{\inf} = (1.60x10^{-20}) * T_{gas}^{-3.47} * e\left(-\frac{475.0}{T_{gas}}\right)$	(5)

	$K_0 = (9.20x10^{-16}) * T_{gas}^{1.64} * e\left(-\frac{1055.0}{T_{gas}}\right)$ $F = 7.94x10^{-4} * T_{gas}^{0.78}$	
$C_3H_7 + H \rightarrow C_3H_8$	$K_{\text{inf}} = (4.00x10^{-19}) * T_{gas}^{-3.00} * e\left(-\frac{600.0}{T_{gas}}\right)$ $K_0 = (2.49x10^{-10})$ $F = (1 - 0.315) * e\left(-\frac{T_{gas}}{369.0}\right) + 0.315 * e\left(-\frac{T_{gas}}{3285}\right) + e\left(-\frac{6667}{T_{gas}}\right)$	(5)
$H + C_2H \rightarrow C_2H_2$	$K_{\text{inf}} = (1.26x10^{-18}) * T_{gas}^{-3.10} * e\left(-\frac{721.0}{T_{gas}}\right)$ $K_0 = (2.31x10^{-10}) * \left(\frac{T_{gas}}{298}\right)^{-0.32}$ $F = (1 - 0.646) * e\left(-\frac{T_{gas}}{132.0}\right) + 0.646 * e\left(-\frac{T_{gas}}{1315}\right) + e\left(-\frac{5566}{T_{gas}}\right)$	(5)
$C_2H_5 \rightarrow C_2H_4 + H$	$(8.20x10^{13}) * e\left(-\frac{20070.0}{T_{gas}}\right)$	(5)
$C_2H_3 \rightarrow C_2H_2 + H$	$3.94x10^{12} * T_{gas}^{1.62} * e\left(-\frac{155000.0}{R_{gas} * T_{gas}}\right)$	(5)
$CH_4 + CH_3 \rightarrow H + C_2H_6$	$4.95x10^{-13} * \left(\frac{T_{gas}}{298.15}\right) * e\left(-\frac{188000.0}{R_{gas} * T_{gas}}\right)$	(5)
$CH_4 + CH_3 \rightarrow H_2 + C_2H_5$	$1.66x10^{-11} * e\left(\frac{-96450.0}{R_{gas} * T_{gas}}\right)$	(5)
$CH_4 + CH_2 \rightarrow CH_3 + CH_3$	$7.14x10^{-12} * e\left(-\frac{41990.0}{R_{gas} * T_{gas}}\right)$	(5)

$CH_4 + CH \rightarrow C_2H_4 + H$	$3.96x10^{-8} * \left(\frac{T_{gas}}{298.15}\right)^{-1.04x10^{0}} * e\left(-\frac{36.1}{T_{gas}}\right)$	(5)
$CH_4 + C \rightarrow CH + CH_3$	$8.30x10^{-11} * e\left(-\frac{24.015}{1.987 * T_{gas}}\right)$	(5)
$CH_4 + C \rightarrow C_2H_4$	$5.00x10^{-15}$	(5)
$CH_4 + C_2H_5 \rightarrow C_2H_6 + CH_3$	$2.51x10^{-15} * \left(\frac{T_{gas}}{298}\right)^{2.84} * e\left(-\frac{52550}{R_{gas} * T_{gas}}\right)$	(5)
$CH_4 + C_2H_3 \rightarrow C_2H_4 + CH_3$	$2.13x10^{-14} * \left(\frac{T_{gas}}{298}\right)^{4.02} * e\left(-\frac{22860}{R_{gas} * T_{gas}}\right)$	(5)
$CH_4 + C_2H \rightarrow C_2H_2 + CH_3$	$3.01x10^{-12} * e\left(-\frac{2080}{R_{gas} * T_{gas}}\right)$	(5)
$CH_4 + C_3H_7 \rightarrow C_3H_8 + CH_3$	$3.54x10^{-16} * \left(\frac{T_{gas}}{298}\right)^{4.02} * e\left(-\frac{45480}{R_{gas} * T_{gas}}\right)$	(5)
$CH_4 + C_3H_5 \rightarrow C_3H_6 + CH_3$	$1.71x10^{-14} * \left(\frac{T_{gas}}{298}\right)^{3.40} * e\left(-\frac{97280}{R_{gas} * T_{gas}}\right)$	(5)
$CH_4 + H \rightarrow CH_3 + H_2$	$4.63x10^{-13} * \left(\frac{T_{gas}}{298}\right)^{3.16} * e\left(-\frac{36630.0}{R_{gas} * T_{gas}}\right)$	(5)
$CH_3 + CH_3 \rightarrow C_2H_5 + H$	$1.46x10^{-11} * \left(\frac{T_{gas}}{298.15}\right)^{0.10} * e\left(-\frac{44400}{R_{gas} * T_{gas}}\right)$	(5)
$CH_3 + CH_3 \rightarrow CH_2 + CH_4$	$1.16x10^{-13} * \left(\frac{T_{gas}}{298.15}\right)^{1.34} * e\left(-\frac{67910.0}{R_{gas} * T_{gas}}\right)$	(5)
$CH_3 + CH_3 \rightarrow C_2H_4 + H_2$	$1.66x10^{-8} * e\left(-\frac{138000.0}{R_{gas} * T_{gas}}\right)$	(5)
$CH_3 + CH_2 \rightarrow C_2H_4 + H$	$5.01x10^{-11}$	(5)
$CH_3 + C_2H_6 \rightarrow C_2H_5 + CH_4$	$1.74x10^{-16} * \left(\frac{T_{gas}}{298}\right)^{6.00} * e\left(-\frac{25280}{R_{gas} * T_{gas}}\right)$	(5)

$CH_3 + C_2H_5 \rightarrow C_2H_4 + CH_4$	$1.88x10^{-12} * \left(\frac{T_{gas}}{298.0}\right)^{-0.5}$	(5)
$CH_3 + C_2H_5 \rightarrow C_2H_6 + CH_2$	$3.0x10^{-44} * \left(T_{gas}\right)^{9.0956}$	(5)
$CH_3 + C_2H_4 \rightarrow C_2H_3 + CH_4$	$6.91x10^{-12} * e\left(-\frac{46560.0}{R_{gas} * T_{gas}}\right)$	(5)
$CH_3 + C_2H_4 \rightarrow C_3H_7$	$3.50x10^{-13} * e\left(-\frac{3700}{T_{gas}}\right)$	(5)
$CH_3 + C_2H_3 \rightarrow C_2H_2 + CH_4$	$1.5x10^{-11} * e\left(\frac{3200.0}{R_{gas} * T_{gas}}\right)$	(5)
$CH_3 + C_2H_3 \rightarrow C_3H_5 + H$	$2.59E-9 * \left(\frac{T_{gas}}{298.0}\right)^{-1.25} * e\left(-\frac{3.21E4}{R_{gas} * T_{gas}}\right)$	(5)
$CH_3 + C_2H_2 \rightarrow CH_4 + C_2H$	$3.01x10^{-13} * e\left(-\frac{72340}{R_{gas} * T_{gas}}\right)$	(5)
$CH_3 + C_2H_2 \rightarrow C_3H_5$	$1.00x10^{-12} * e\left(-\frac{3900}{T_{gas}}\right)$	(5)
$CH_3 + C_3H_8 \rightarrow C_3H_7 + CH_4$	$1.499x10^{-24} * \left(T_{gas}\right)^{3.65} * e\left(-\frac{7154.0}{1.987 * T_{gas}}\right)$	(5)
$CH_3 + C_3H_7 \rightarrow C_3H_6 + CH_4$	$3.07x10^{-12} * \left(\frac{T_{gas}}{298}\right)^{-0.32}$	(5)
$CH_3 + C_3H_7 \rightarrow C_2H_5 + C_2H_5$	$\left(\frac{1.93x10^{13}}{6.0223E23}\right) * \left(T_{gas}\right)^{-0.32}$	(5)
$CH_3 + C_3H_6 \rightarrow C_3H_5 + CH_4$	$1.68x10^{-15} * \left(\frac{T_{gas}}{298}\right)^{3.50} * e\left(-\frac{23780}{R_{gas} * T_{gas}}\right)$	(5)
$CH_3 + H \rightarrow CH_2 + H_2$	$1.00x10^{-10} * e\left(-\frac{63190}{R_{gas} * T_{gas}}\right)$	(5)
$CH_3 \rightarrow H_2 + CH$	$8.30x10^{-9} * e\left(-\frac{356000.0}{R_{gas} * T_{gas}}\right)$	(5)

$CH_3 \rightarrow CH_2 + H$	$1.69x10^{-8} * e\left(-\frac{379000.0}{R_{gas} * T_{gas}}\right)$	(5)
$CH_2 + CH_2 \rightarrow C_2H_2 + H + H$	$3.32x10^{-10} * e\left(-\frac{45980.0}{R_{gas} * T_{gas}}\right)$	(5)
$CH_2 + CH_2 \rightarrow C_2H_2 + H_2$	$2.62x10^{-9} * e\left(-\frac{49970.0}{R_{gas} * T_{gas}}\right)$	(5)
$CH_2 + CH_3 \rightarrow C_2H_5$	$7.00x10^{-23} * T_{gas}^{3.6337}$	(5)
$CH_2 + C_2H_6 \rightarrow C_2H_5 + CH_3$	$9.0x10^{-33} * \left(T_{gas}\right)^{6.4162}$	(5)
$CH_2 + C_2H_6 \rightarrow C_3H_8$	$4.80E-12$	(5)
$CH_2 + C_2H_5 \rightarrow C_2H_4 + CH_3$	$8.01x10^{-11}$	(5)
$CH_2 + C_2H_3 \rightarrow C_2H_2 + CH_3$	$8.01x10^{-11}$	(5)
$CH_2 + C_2H_4 \rightarrow C_3H_5 + H$	$4.25x10^{-12} * e\left(-\frac{2658}{T_{gas}}\right)$	(5)
$CH_2 + C_2H \rightarrow C_2H_2 + CH$	$3.01x10^{-11}$	(5)
$CH_2 + C_3H_8 \rightarrow C_3H_7 + CH_3$	$1.61x10^{-15} * \left(\frac{T_{gas}}{298}\right)^{3.65} * e\left(-\frac{29930}{R_{gas} * T_{gas}}\right)$	(5)
$CH_2 + C_3H_7 \rightarrow C_2H_4 + C_2H_5$	$3.01x10^{-11}$	(5)
$CH_2 + C_3H_7 \rightarrow C_3H_6 + CH_3$	$3.01x10^{-11}$	(5)
$CH_2 + C_3H_6 \rightarrow C_3H_5 + CH_3$	$1.20x10^{-12} * e\left(-\frac{25940}{R_{gas} * T_{gas}}\right)$	(5)
$CH_2 + H_2 \rightarrow CH_3 + H$	$3.59x10^{-13} * \left(\frac{T_{gas}}{298}\right)^{2.30} * e\left(-\frac{30760.0}{R_{gas} * T_{gas}}\right)$	(5)

$CH_2 + H \rightarrow CH + H_2$	$1.00x10^{-11} * e\left(\frac{7480}{R_{gas} * T_{gas}}\right)$	(5)
$CH_2 \rightarrow C + H_2$	$5.00x10^{-10} * e\left(-\frac{32600.0}{T_{gas}}\right)$	(5)
$CH_2 \rightarrow CH + H$	$1.56x10^{-8} * e\left(-\frac{44880.0}{T_{gas}}\right)$	(5)
$CH + H_2 \rightarrow CH_2 + H$	$1.48x10^{-11} * \left(\frac{T_{gas}}{298.0}\right)^{1.79} * e\left(-\frac{6980.0}{R_{gas} * T_{gas}}\right)$	(5)
$CH + H \rightarrow C + H_2$	$6.50x10^{-10} * \left(T_{gas}^{0.01}\right) * e\left(-\frac{22330.0}{R_{gas} * T_{gas}}\right)$	(5)
$CH + CH_3 \rightarrow C_2H_3 + H$	$\left(3\frac{x10^{13}}{6.0223E23}\right)$	(5)
$CH + CH_2 \rightarrow C_2H_2 + H$	$\left(4\frac{x10^{13}}{6.0223E23}\right)$	(5)
$CH + CH \rightarrow C_2H_2$	$1.99\ x10^{-10}$	(5)
$CH + C_2H_2 \rightarrow C_2H + CH_2$	$3.80x10^{-8} * \left(T_{gas}^{-0.859}\right) * e\left(-\frac{33.5}{T_{gas}}\right)$	(5)
$CH + C_2H_3 \rightarrow CH_2 + C_2H_2$	$8.30\ x10^{-11}$	(5)
$CH + C_2H_4 \rightarrow C_3H_5$	$2.84x10^{-10} * \left(\frac{T_{gas}}{298.15}\right)^{-0.310}$	(5)
$CH + C_2H_4 \rightarrow C_2H_2 + CH_3$	$0.50\ *\ 1.59x10^{-9} * \left(T_{gas}^{-0.546}\right) * e\left(-\frac{29.6}{T_{gas}}\right)$	(5)
$CH + C_2H_4 \rightarrow CH_4 + C_2H$	$0.50\ *\ 1.59x10^{-9} * \left(T_{gas}^{-0.546}\right) * e\left(-\frac{29.6}{T_{gas}}\right)$	(5)
$CH + C_2H_5 \rightarrow C_3H_5 + H$	$3.80x10^{-8} * \left(T_{gas}^{-0.859}\right) * e\left(-\frac{33.5}{T_{gas}}\right)$	(5)

$CH + C_2H_6 \rightarrow C_2H_4 + CH_3$	$3.80x10^{-8} * \left(T_{gas}^{-0.859}\right) * e\left(-\frac{53.2}{T_{gas}}\right)$	(5)
$CH + C_2H_6 \rightarrow C_3H_6 + H$	$6.17x10^{-11} * \left(T_{gas}^{-0.52}\right) * e\left(-\frac{29.2}{T_{gas}}\right)$	(5)
$CH + C_2H_6 \rightarrow C_3H_7$	$1.60x10^{-10}$	(5)
$CH \rightarrow C + H$	$3.16x10^{-10} * e\left(-\frac{280000.0}{R_{gas} * T_{gas}}\right)$	(5)
$C_2H_6 + C_2H_3 \rightarrow C_2H_5 + C_2H_4$	$1.46x10^{-13} * \left(\frac{T_{gas}}{298}\right)^{3.30} * e\left(-\frac{43900.0}{R_{gas} * T_{gas}}\right)$	(5)
$C_2H_6 + C_2H \rightarrow C_2H_2 + C_2H_5$	$3.50x10^{-11} * e\left(\frac{20.0}{R_{gas} * T_{gas}}\right)$	(5)
$C_2H_6 + C_3H_7 \rightarrow C_3H_8 + C_2H_5$	$1.19x10^{-15} * \left(\frac{T_{gas}}{298}\right)^{3.82} * e\left(-\frac{37830}{R_{gas} * T_{gas}}\right)$	(5)
$C_2H_6 + C_3H_5 \rightarrow C_3H_6 + C_2H_5$	$5.71x10^{-14} * \left(\frac{T_{gas}}{298}\right)^{3.30} * e\left(-\frac{83060}{R_{gas} * T_{gas}}\right)$	(5)
$C_2H_6 + H \rightarrow C_2H_5 + H_2$	$1.23x10^{-11} * \left(\frac{T_{gas}}{298}\right)^{1.50} * e\left(-\frac{31010}{R_{gas} * T_{gas}}\right)$	(5)
$H + C_2H_6 \rightarrow CH_4 + CH_3$	$8.97x10^{-20} * e\left(-\frac{48640.0}{R_{gas} * T_{gas}}\right)$	(5)
$C_2H_6 \rightarrow C_2H_5 + H$	$8.11x10^{17} * \left(\frac{T_{gas}}{298.15}\right)^{-1.23} * e\left(-\frac{427000.0}{R_{gas} * T_{gas}}\right)$	(5)
$C_2H_6 \rightarrow C_2H_4 + H_2$	$1.32x10^{15} * e\left(-\frac{306000.0}{R_{gas} * T_{gas}}\right)$	(5)
$C_2H_5 + C_2H_3 \rightarrow C_2H_6 + C_2H_2$	$0.369 * 6.50x10^{-11}$	(5)
$C_2H_5 + C_2H_3 \rightarrow C_2H_4 + C_2H_4$	$8.00x10^{-15} * e\left(0.0024 * T_{gas}\right) + 0.68 * 6.5x10^{-11}$	(5)

$C_2H_5 + C_2H_5 \rightarrow C_2H_6 + C_2H_4$	$2.41x10^{-12}$	(5)
$C_2H_5 + C_2H_4 \rightarrow C_2H_6 + C_2H_3$	$5.83x10^{-14} * \left(\frac{T_{gas}}{298.15}\right)^{3.13} * e\left(-\frac{75330}{R_{gas} * T_{gas}}\right)$	(5)
$C_2H_5 + C_2H_2 \rightarrow C_2H_6 + C_2H$	$4.50x10^{-13} * e\left(-\frac{98110}{R_{gas} * T_{gas}}\right)$	(5)
$C_2H_5 + C_2H \rightarrow C_2H_4 + C_2H_2$	$3.01x10^{-12}$	(5)
$C_2H_5 + C_3H_8 \rightarrow C_2H_6 + C_3H_7$	$1.61x10^{-15} * \left(\frac{T_{gas}}{298.15}\right)^{3.65} * e\left(-\frac{38250}{R_{gas} * T_{gas}}\right)$	(5)
$C_2H_5 + C_3H_7 \rightarrow C_3H_8 + C_2H_4$	$1.91x10^{-12}$	(5)
$C_2H_5 + C_3H_7 \rightarrow C_3H_6 + C_2H_6$	$2.41x10^{-12}$	(5)
$C_2H_5 + C_3H_6 \rightarrow C_3H_5 + C_2H_6$	$1.69x10^{-15} * \left(\frac{T_{gas}}{298.15}\right)^{3.50} * e\left(-\frac{27770}{R_{gas} * T_{gas}}\right)$	(5)
$C_2H_5 + C_3H_5 \rightarrow C_3H_6 + C_2H_4$	$4.30x10^{-12} * e\left(\frac{550.0}{R_{gas} * T_{gas}}\right)$	(5)
$C_2H_5 + H_2 \rightarrow C_2H_6 + H$	$5.10x10^{-24} * \left(\frac{T_{gas}}{298.15}\right)^{3.60} * e\left(-\frac{35340.0}{R_{gas} * T_{gas}}\right)$	(5)
$H + C_2H_5 \rightarrow CH_3 + CH_3$	$1.79x10^{-10} * e\left(-\frac{3640.0}{R_{gas} * T_{gas}}\right)$	(5)
$H + C_2H_5 \rightarrow C_2H_4 + H_2$	$3.321x10^{-12}$	(5)
$C_2H_5 \rightarrow CH_2 + CH_3$	$1.0x10^{-118} * T_{gas}^{37.47}$	(5)
$C_2H_4 + C_2H \rightarrow C_2H_2 + C_2H_3$	$1.40x10^{-10}$	(5)
$C_2H_4 + C_2H_2 \rightarrow C_2H_3 + C_2H_3$	$4.0x10^{-11} * e\left(-\frac{286000.0}{R_{gas} * T_{gas}}\right)$	(5)

$C_2H_4 + C_3H_6 \rightarrow C_3H_5 + C_2H_5$	$9.6x10^{-11} * e\left(-\frac{216000.0}{R_{gas} * T_{gas}}\right)$	(5)
$C_2H_4 + C_3H_6 \rightarrow C_2H_3 + C_3H_7$	$1.0x10^{-10} * e\left(-\frac{316000.0}{R_{gas} * T_{gas}}\right)$	(5)
$C_2H_4 + C_2H_4 \rightarrow C_2H_5 + C_2H_3$	$\left(\frac{1}{1.0}\right) * 8.0x10^{-10} * e\left(-\frac{299000.0}{R_{gas} * T_{gas}}\right)$	(5)
$C_2H_4 + H \rightarrow C_2H_3 + H_2$	$8.41x10^{-17} * \left(T_{gas}\right)^{1.93} * e\left(-\frac{6518}{T_{gas}}\right)$	(5)
$C_2H_4 + H_2 \rightarrow C_2H_6$	$4.75x10^{-16} * e\left(-\frac{180000.0}{R_{gas} * T_{gas}}\right)$	(5)
$C_2H_4 + C \rightarrow C_2H_2 + CH_2$	$1.24x10^{-11}$	(5)
$C_2H_4 \rightarrow C_2H_3 + H$	$2.00E16 * e\left(-\frac{461000.0}{R_{gas} * T_{gas}}\right)$	(5)
$C_2H_3 + C_2H_3 \rightarrow C_2H_4 + C_2H_2$	$3.50x10^{-11}$	(5)
$C_2H_3 + C_2H \rightarrow C_2H_2 + C_2H_2$	$3.15x10^{-11}$	(5)
$C_2H_3 + C_3H_8 \rightarrow C_2H_4 + C_3H_7$	$1.46x10^{-13} * \left(\frac{T_{gas}}{298}\right)^{3.30} * e\left(-\frac{43900}{R_{gas} * T_{gas}}\right)$	(5)
$C_2H_3 + C_3H_7 \rightarrow C_3H_8 + C_2H_2$	$2.01x10^{-12}$	(5)
$C_2H_3 + C_3H_7 \rightarrow C_3H_6 + C_2H_4$	$2.01x10^{-12}$	(5)
$C_2H_3 + C_3H_6 \rightarrow C_3H_5 + C_2H_4$	$1.68x10^{-15} * \left(\frac{T_{gas}}{298}\right)^{3.50} * e\left(-\frac{19620}{R_{gas} * T_{gas}}\right)$	(5)
$C_2H_3 + C_3H_5 \rightarrow C_3H_6 + C_2H_2$	$8.00x10^{-12}$	(5)
$C_2H_3 + H \rightarrow C_2H_2 + H_2$	$1.50x10^{-12} * \left(T_{gas}\right)^{0.50}$	(5)

$C_2H_2 + C_3H_7 \rightarrow C_3H_5 + C_2H_4$	$1.20E-12 * e\left(-\frac{3.77E4}{R_{gas} * T_{gas}}\right)$	(5)
$C_2H_2 + C_3H_6 \rightarrow C_2H_3 + C_3H_5$	$6.71x10^{-11} * e\left(-\frac{196000.0}{R_{gas} * T_{gas}}\right)$	(5)
$C_2H_2 + C_2H_2 \rightarrow C_2H + C_2H_3$	$1.6x10^{-11} * e\left(-\frac{353000.0}{R_{gas} * T_{gas}}\right)$	(5)
$C_2H_2 + H_2 \rightarrow C_2H_4$	$5.0x10^{-13} * e\left(-\frac{163000.0}{R_{gas} * T_{gas}}\right)$	(5)
$C_2H_2 + H \rightarrow C_2H + H_2$	$2.77x10^{-10} * \left(\frac{T_{gas}}{298.0}\right)^{1.32} * e\left(-\frac{128000}{R_{gas} * T_{gas}}\right)$	(5)
$C_2H_2 \rightarrow C_2H + H$	$2.63x10^{15} * e\left(-\frac{519000.0}{R_{gas} * T_{gas}}\right)$	(5)
$C_2H + C_3H_8 \rightarrow C_2H_2 + C_3H_7$	$1.789x10^{-11}$	(5)
$C_2H + C_3H_7 \rightarrow C_3H_6 + C_2H_2$	$2.01x10^{-11}$	(5)
$C_2H + C_3H_6 \rightarrow C_3H_5 + C_2H_2$	$1.789x10^{-11}$	(5)
$C_2H + C_2H \rightarrow C_2H_2 + C_2$	$3.01x10^{-12}$	(5)
$C_3H_8 + C_3H_5 \rightarrow C_3H_6 + C_3H_7$	$5.71x10^{-14} * \left(\frac{T_{gas}}{298}\right)^{3.30} * e\left(-\frac{83060}{R_{gas} * T_{gas}}\right)$	(5)
$C_3H_8 + H \rightarrow C_3H_7 + H_2$	$4.23x10^{-12} * \left(\frac{T_{gas}}{298}\right)^{2.54} * e\left(-\frac{28270}{R_{gas} * T_{gas}}\right)$	(5)
$C_3H_8 \rightarrow C_3H_7 + H$	$1.58x10^{16} * e\left(-\frac{408000.0}{R_{gas} * T_{gas}}\right)$	(5)
$C_3H_7 + C_3H_7 \rightarrow C_3H_6 + C_3H_8$	$2.81x10^{-12}$	(5)

$C_3H_7 + C_3H_6 \rightarrow C_3H_5 + C_3H_8$	$1.69x10^{-15} * \left(\frac{T_{gas}}{298}\right)^{3.50} * e\left(-\frac{27770}{R_{gas} * T_{gas}}\right)$	(5)
$C_3H_7 + C_3H_5 \rightarrow C_3H_6 + C_3H_6$	$2.41x10^{-12} * e\left(\frac{550}{R_{gas} * T_{gas}}\right)$	(5)
$C_3H_7 + H \rightarrow C_3H_6 + H_2$	$3.01x10^{-12}$	(5)
$C_3H_7 + H \rightarrow CH_3 + C_2H_5$	$6.742x10^{-18} * \left(\left(T_{gas}\right)^{2.19}\right) * e\left(-\frac{890.0}{1.987 * T_{gas}}\right)$	(5)
$C_3H_7 \rightarrow C_2H_4 + CH_3$	$1.31x10^{13} * \left(\frac{T_{gas}}{298.15}\right)^{0.87} * e\left(-\frac{127000.0}{R_{gas} * T_{gas}}\right)$	(5)
$C_3H_6 + C_3H_6 \rightarrow C_3H_7 + C_3H_5$	$4.2x10^{-10} * e\left(-\frac{231000.0}{R_{gas} * T_{gas}}\right)$	(5)
$C_3H_6 + H \rightarrow C_3H_5 + H_2$	$4.40x10^{-13} * \left(\frac{T_{gas}}{298}\right)^{2.50} * e\left(-\frac{10390}{R_{gas} * T_{gas}}\right)$	(5)
$C_3H_6 + H \rightarrow C_2H_4 + CH_3$	$7.51x10^{-11} * e\left(-\frac{17300}{R_{gas} * T_{gas}}\right)$	(5)
$C_3H_6 \rightarrow C_3H_5 + H$	$2.50x10^{15} * e\left(\frac{-410000.0}{R_{gas} * T_{gas}}\right)$	(5)
$C_3H_6 \rightarrow CH_3 + C_2H_3$	$1.18x10^{18} * \left(\frac{T_{gas}}{298.15}\right)^{-1.20} * e\left(-\frac{409000.0}{R_{gas} * T_{gas}}\right)$	(5)
$C_3H_6 \rightarrow CH_4 + C_2H_2$	$3.50x10^{12} * e\left(\frac{-293000.0}{R_{gas} * T_{gas}}\right)$	(5)
$C_3H_6 \rightarrow CH_2 + C_2H_4$	$5.03x10^{15} * e\left(\frac{-808000.0}{R_{gas} * T_{gas}}\right)$	(5)
$C_3H_5 + H \rightarrow C_2H_3 + CH_3$	$4.00x10^{-12}$	(5)
$C_3H_5 \rightarrow C_2H_2 + CH_3$	$1.26x10^{13} * e\left(-\frac{140000.0}{R_{gas} * T_{gas}}\right)$	(5)

$C + C \rightarrow C_2$	$2.20x10^{-11}$	(5)
$C_2 + C_2 \rightarrow C + C_3$	$5.31x10^{-10}$	(5)
$C + CH_2 \rightarrow CH + CH$	$2.69x10^{-12} * e\left(-\frac{196000.0}{R_{gas} * T_{gas}}\right)$	(5)
$C + CH_2 \rightarrow H + C_2H$	$8.30x10^{-11}$	(5)
$C + CH_3 \rightarrow H + C_2H_2$	$8.30x10^{-11}$	(5)
$C_2 + H_2 \rightarrow C_2H_2$	$1.77x10^{-11} * e\left(-\frac{1470.0}{T_{gas}}\right)$	(5)
$C_2 + H_2 \rightarrow C_2H + H$	$1.10x10^{-10} * e\left(-\frac{33260.0}{R_{gas} * T_{gas}}\right)$	(5)
$C_2 + CH_4 \rightarrow C_2H + CH_3$	$5.05x10^{-11} * e\left(-\frac{297}{T_{gas}}\right)$	(5)
$C_3H_7 \rightarrow C_3H_6 + H$	$K_{\inf} = (3.56x10^{-7}) * e\left(-\frac{14200.0}{T_{gas}}\right)$ $K_0 = (8.76x10^{7}) * T_{gas}^{1.76} * e\left(-\frac{17870.0}{T_{gas}}\right)$ $F = 0.35x10^{0}$	(5)
$C_3H_8 \rightarrow C_2H_5 + CH_3$	$K_{\inf} = (1.30x10^{-5}) * e\left(-\frac{32700.0}{T_{gas}}\right)$ $K_0 = (4.00x10^{23}) * T_{gas}^{-1.87} * e\left(-\frac{45394.0}{T_{gas}}\right)$ $F = (0.24) * e\left(-\frac{T_{gas}}{1946.0}\right) + 0.76 * e\left(-\frac{T_{gas}}{38}\right)$	(5)
$H + H \rightarrow H_2$	$K_{\inf} = \left(\frac{1.0}{0.64}\right) * (2.70x10^{-31}) * T_{gas}^{-0.60}$	(5)

	$K_0 = (1.11x10^{-08}) * \left(\frac{T_{gas}}{298}\right)^{-1.00}$ $F = (0.0506) * T_{gas}^{0.40}$	
$CH_3 + C_2H_3 \rightarrow C_3H_6$	$K_{\inf} = (5.00x10^{-27})$ $K_0 = (1.10x10^{-10})$ $F = (0.0506) * T_{gas}^{0.40}$	(5)
$CH_2 + C_2H_4 \rightarrow C_3H_6$	$K_{\inf} = (1.5x10^{-18}) * T_{gas}^{-3} * e\left(-\frac{300}{T_{gas}}\right)$ $K_0 = (9.17x10^{-12}) * \left(\frac{T_{gas}}{298.15}\right)^{0.00730} * e\left(-\frac{4410.0}{R_{gas} * T_{gas}}\right)$ $F = (0.0506) * T_{gas}^{0.40}$	(5)
$C + H_2 \rightarrow CH_2$	$K_{\inf} = \left(\frac{1.0}{0.64}\right) * (7.00x10^{-32})$ $K_0 = (2.06x10^{-11}) * e\left(-\frac{57}{T_{gas}}\right)$ $F = (0.0506) * T_{gas}^{0.40}$	(5)
$C_3H_6 + H \rightarrow C_3H_7$	$K_{\inf} = (1.30x10^{-28}) * e\left(-\frac{380}{T_{gas}}\right)$ $K_0 = (9.47x10^{-15}) * T_{gas}^{1.16} * e\left(-\frac{440.0}{T_{gas}}\right)$ $F = (0.0506) * T_{gas}^{0.40}$	(5)
$C_3H_5 + H \rightarrow C_3H_6$	$K_{\inf} = (1.50x10^{-29})$ $K_0 = (2.4x10^{-10})$ $F = (0.0506) * T_{gas}^{0.40}$	(5)

$CH + N_2 \rightarrow CN_2H$	$K_{\inf} = (4.4x10^{-26}) * T_{gas}^{-2.2}$ $K_0 = (9.6x10^{-11}) * e\left(-\frac{0.15}{T_{gas}}\right)$ $F = e\left(-\frac{T_{gas}}{660}\right) + e\left(-\frac{1080}{T_{gas}}\right)$	(5)

Table 2. Electron impact reactions (described by cross sections) in the model chemistry set.

$e^- + HCN \rightarrow HCN^+ + e^- + e^-$	(7)
$e^- + NH_4^+ \rightarrow NH_2 + H + H$	(7)
$e^- + NH_4^+ \rightarrow NH_2 + H_2$	(7)
$e^- + NH_3^+ \rightarrow NH + H + H$	(7)
$e^- + NH_3^+ \rightarrow NH_2 + H$	(7)
$HCN^+ + e^- \rightarrow CN + H$	(7)
$e^- + NH_2 \rightarrow NH_2^+ + e^- + e^-$	(7)
$e^- + NH_2^+ \rightarrow NH + H$	(7)
$e^- + NH_2^+ \rightarrow N + H + H$	(7)
$e^- + NH \rightarrow NH^+ + e^- + e^-$	(7)
$e^- + NH^+ \rightarrow N + H$	(7)
$e^- + N \rightarrow N^+ + e^- + e^-$	(7)
$e^- + N_2 \rightarrow e^- + N + N$	(7)
$e^- + NH \rightarrow H + N^+ + e^- + e^-$	(7)
$e^- + N^+ + e^- \rightarrow N + e^-$	(7)

$e^- + N^+ + M \rightarrow N + M$	(7)
$e^- + N_2 \rightarrow e^- + e^- + N^+ + N$	(7)
$e^- + NH_3 \rightarrow NH^+ + H_2 + e^- + e^-$	(7)
$e^- + NH_3 \rightarrow N^+ + H_2 + H + e^- + e^-$	(7)
$e^- + NH_3 \rightarrow NH_2 + H^+ + e^- + e^-$	(7)
$e^- + NH_3 \rightarrow NH + H_2^+ + e^- + e^-$	(7)
$e^- + NH_2 \rightarrow NH + H^+ + e^- + e^-$	(7)
$e^- + NH_2 \rightarrow N^+ + H_2 + e^- + e^-$	(7)
$e^- + NH_3 \rightarrow e^- + NH_2 + H$ *equal cross section of NH_3 (e1)*	(4)
$e^- + NH_3 \rightarrow e^- + NH + H_2$ *equal cross section of NH_3 (e2)*	(4)
$e^- + NH_3 \rightarrow NH_3^+ + e^- + e^-$	(7)
$e^- + NH_3 \rightarrow H + NH_2^+ + e^- + e^-$	(7)
$e^- + NH_4^+ \rightarrow NH_3 + H$	(7)
$e^- + NH_2 \rightarrow e^- + N + H_2$	(7)
$e^- + NH_2 \rightarrow e^- + NH + H$	(7)
$e^- + NH_2 \rightarrow H + NH^+ + e^- + e^-$	(7)
$e^- + NH \rightarrow e^- + N + H$	(7)
$e^- + C_2 \rightarrow e^- + C + C$	(5)
$e^- + C_3 \rightarrow e^- + C_2 + C$	(5)
$e^- + C_3 \rightarrow e^- + C + C + C$	(5)

$e^- + H_2 \rightarrow e^- + H + H$	(5)
$e^- + H_2 \rightarrow e^- + e^- + H_2^+$	(5)
$e^- + H \rightarrow e^- + e^- + H^+$	(5)
$e^- + H_3^+ \rightarrow H_2 + H$	(5)
$e^- + H_3^+ \rightarrow e^- + H_2 + H^+$	(5)
$e^- + H_3^+ \rightarrow H + H + H$	(5)
$e^- + H_2^+ \rightarrow e^- + H + H^+$	(5)
$e^- + H_3^+ \rightarrow e^- + H + H + H^+$	(5)
$e^- + H_2^+ \rightarrow H + H$	(5)
$e^- + CH_4 \rightarrow e^- + e^- + CH_4^+$	(5)
$e^- + CH_4 \rightarrow e^- + e^- + CH_3^+ + H$	(5)
$e^- + CH_4 \rightarrow e^- + e^- + H_2^+ + CH_2$	(5)
$e^- + CH_4 \rightarrow e^- + e^- + H^+ + CH_3$	(5)
$e^- + CH_4 \rightarrow e^- + C + H_2 + H_2$	(5)
$e^- + CH_4 \rightarrow e^- + C + H_2 + H + H$	(5)
$e^- + CH_4 \rightarrow e^- + CH_2 + H_2$	(5)
$e^- + CH_4 \rightarrow e^- + CH_2 + H + H$	(5)
$e^- + CH_4 \rightarrow e^- + CH_3 + H$	(5)
$e^- + CH_4 \rightarrow e^- + CH + H_2 + H$	(5)
$e^- + CH_3 \rightarrow e^- + e^- + CH_3^+$	(5)
$e^- + CH_3 \rightarrow e^- + e^- + H^+ + CH_2$	(5)

$e^- + CH_3 \rightarrow e^- + CH_2 + H$	(5)
$e^- + CH_3 \rightarrow e^- + CH + H_2$	(5)
$e^- + CH_3 \rightarrow e^- + C + H_2 + H$	(5)
$e^- + CH_3 \rightarrow e^- + CH + H + H$	(5)
$e^- + CH_2 \rightarrow e^- + e^- + H_2^+ + C$	(5)
$e^- + CH_2 \rightarrow e^- + e^- + H^+ + CH$	(5)
$e^- + CH_2 \rightarrow e^- + CH + H$	(5)
$e^- + CH_2 \rightarrow e^- + C + H_2$	(5)
$e^- + CH_2 \rightarrow e^- + C + H + H$	(5)
$e^- + CH \rightarrow e^- + e^- + C + H^+$	(5)
$e^- + CH \rightarrow e^- + C + H$	(5)
$e^- + C_2H_6 \rightarrow e^- + C_2H_5 + H$	(5)
$e^- + C_2H_6 \rightarrow e^- + C_2H_4 + H_2$	(5)
$e^- + C_2H_6 \rightarrow e^- + C_2H_3 + H_2 + H$	(5)
$e^- + C_2H_6 \rightarrow e^- + C_2H_2 + H_2 + H_2$	(5)
$e^- + C_2H_6 \rightarrow e^- + CH_4 + CH_2$	(5)
$e^- + C_2H_6 \rightarrow e^- + CH_3 + CH_3$	(5)
$e^- + C_2H_6 \rightarrow e^- + e^- + CH_3^+ + CH_3$	(5)
$e^- + C_2H_6 \rightarrow e^- + e^- + H_2^+ + C_2H_4$	(5)
$e^- + C_2H_5 \rightarrow e^- + C_2H_4 + H$	(5)
$e^- + C_2H_5 \rightarrow e^- + C_2H_3 + H_2$	(5)

$e^- + C_2H_5 \rightarrow e^- + C_2H_3 + H + H$	(5)
$e^- + C_2H_5 \rightarrow e^- + C_2H_2 + H_2 + H$	(5)
$e^- + C_2H_5 \rightarrow e^- + C_2H + H_2 + H_2$	(5)
$e^- + C_2H_5 \rightarrow e^- + CH_4 + CH$	(5)
$e^- + C_2H_5 \rightarrow e^- + CH_3 + CH_2$	(5)
$e^- + C_2H_5 \rightarrow e^- + e^- + CH_3^+ + CH_2$	(5)
$e^- + C_2H_4 \rightarrow e^- + C_2H_3 + H$	(5)
$e^- + C_2H_4 \rightarrow e^- + C_2H_2 + H_2$	(5)
$e^- + C_2H_4 \rightarrow e^- + C_2H + H_2 + H$	(5)
$e^- + C_2H_4 \rightarrow e^- + CH_3 + CH$	(5)
$e^- + C_2H_4 \rightarrow e^- + CH_2 + CH_2$	(5)
$e^- + C_2H_4 \rightarrow e^- + C + CH_4$	(5)
$e^- + C_2H_4 \rightarrow e^- + e^- + CH_3^+ + CH$	(5)
$e^- + C_2H_3 \rightarrow e^- + C_2H_2 + H$	(5)
$e^- + C_2H_3 \rightarrow e^- + C_2H + H + H$	(5)
$e^- + C_2H_3 \rightarrow e^- + C_2 + H_2 + H$	(5)
$e^- + C_2H_3 \rightarrow e^- + CH_2 + CH$	(5)
$e^- + C_2H_3 \rightarrow e^- + C + CH_3$	(5)
$e^- + C_2H_3 \rightarrow e^- + e^- + H^+ + C_2H_2$	(5)
$e^- + C_2H_2 \rightarrow e^- + C_2H + H$	(5)
$e^- + C_2H_2 \rightarrow e^- + C + CH_2$	(5)

$e^- + C_2H_2 \rightarrow e^- + CH + CH$	(5)
$e^- + C_2H_2 \rightarrow e^- + C_2 + H_2$	(5)
$e^- + C_2H_2 \rightarrow e^- + C_2 + H + H$	(5)
$e^- + C_2H_2 \rightarrow e^- + e^- + H^+ + C_2H$	(5)
$e^- + C_2H \rightarrow e^- + C_2 + H$	(5)
$e^- + C_2H \rightarrow e^- + C + CH$	(5)
$e^- + CH_3^+ \rightarrow C + H_2 + H$	(5)
$e^- + CH_3^+ \rightarrow CH_2 + H$	(5)
$e^- + CH_3^+ \rightarrow CH + H_2$	(5)
$e^- + CH_3^+ \rightarrow CH + H + H$	(5)
$e^- + CH_3^+ \rightarrow e^- + H_2^+ + C + H$	(5)
$e^- + CH_3^+ \rightarrow e^- + H_2^+ + CH$	(5)
$e^- + CH_3^+ \rightarrow e^- + H^+ + C + H_2$	(5)
$e^- + CH_3^+ \rightarrow e^- + H^+ + CH_2$	(5)
$e^- + CH_3^+ \rightarrow e^- + H^+ + CH + H$	(5)
$e^- + CH_4^+ \rightarrow CH_2 + H + H$	(5)
$e^- + CH_4^+ \rightarrow CH_3 + H$	(5)
$e^- + CH_4^+ \rightarrow CH + H_2 + H$	(5)
$e^- + CH_4^+ \rightarrow C + H_2 + H_2$	(5)
$e^- + CH_4^+ \rightarrow CH_2 + H_2$	(5)
$e^- + CH_4^+ \rightarrow e^- + CH_3^+ + H$	(5)

$e^- + CH_4^+ \rightarrow e^- + e^- + CH_3^+ + H^+$	(5)
$e^- + CH_4^+ \rightarrow e^- + H_2^+ + C + H_2$	(5)
$e^- + CH_4^+ \rightarrow e^- + H_2^+ + C + H + H$	(5)
$e^- + CH_4^+ \rightarrow e^- + H_2^+ + CH_2$	(5)
$e^- + CH_4^+ \rightarrow e^- + H_2^+ + CH + H$	(5)
$e^- + CH_4^+ \rightarrow e^- + H_3^+ + CH$	(5)
$e^- + CH_4^+ \rightarrow e^- + H^+ + CH_2 + H$	(5)
$e^- + CH_4^+ \rightarrow e^- + H^+ + CH_3$	(5)
$e^- + CH_4^+ \rightarrow e^- + H^+ + CH + H_2$	(5)
$e^- + CH_5^+ \rightarrow CH_3 + H + H$	(5)
$e^- + CH_5^+ \rightarrow CH_2 + H_2 + H$	(5)
$e^- + CH_5^+ \rightarrow CH_3 + H_2$	(5)
$e^- + CH_5^+ \rightarrow CH_4 + H$	(5)
$e^- + C_3H_7 \rightarrow e^- + e^- + CH_3^+ + C_2H_4$	(5)
$e^- + C_3H_6 \rightarrow e^- + e^- + CH_3^+ + C_2H_3$	(5)
$e^- + C_3H_5 \rightarrow e^- + e^- + CH_3^+ + C_2H_2$	(5)
$e^- + C_3H_8 \rightarrow e^- + C_3H_7 + H$	(5)
$e^- + C_3H_8 \rightarrow e^- + C_3H_6 + H_2$	(5)
$e^- + C_3H_8 \rightarrow e^- + C_2H_4 + CH_4$	(5)
$e^- + C_3H_8 \rightarrow e^- + C_2H_6 + CH_2$	(5)
$e^- + C_3H_8 \rightarrow e^- + C_2H_5 + CH_3$	(5)

$e^- + C_3H_7 \rightarrow e^- + C_3H_6 + H$	(5)
$e^- + C_3H_7 \rightarrow e^- + C_2H_4 + CH_3$	(5)
$e^- + C_3H_7 \rightarrow e^- + C_2H_3 + CH_4$	(5)
$e^- + C_3H_7 \rightarrow e^- + C_3H_5 + H_2$	(5)
$e^- + C_3H_6 \rightarrow e^- + C_2H_2 + CH_4$	(5)
$e^- + C_3H_6 \rightarrow e^- + C_3H_5 + H$	(5)
$e^- + C_3H_6 \rightarrow e^- + C_2H_3 + CH_3$	(5)
$e^- + C_3H_6 \rightarrow e^- + C_2H_4 + CH_2$	(5)
$e^- + C_3H_5 \rightarrow e^- + C_2H_2 + CH_3$	(5)
$e^- + C_3H_5 \rightarrow e^- + C_2H + CH_4$	(5)

Appendix references

1. *Ammonia decomposition in a dielectric barrier discharge plasma: Insights from experiments and kinetic modelling.* J.A. Andersen a, K. van 't Veer b, J.M. Christensen a, M. Østberg c, A. Bogaerts b, A.D. Jensen a. 2022. Chemical Engineering Science, Vol. 271, https://doi.org/10.1016/j.ces.2023.118550.

2. *NIST Chemical Kinetics Database. Kinetics Database Resources.* [Online] https://kinetics.nist.gov/kinetics/index.jsp.

3. *The UMIST Database for Astrochemistry.* [Online] http://udfa.ajmarkwick.net/.

4. *Kinetic Study for Plasma Assisted Cracking of NH3: Approaches and Challenges.* Seunghwan Bang, Ramses Snoeckx, and Min Suk Cha. 2023. J. Phys. Chem. A, Vol. 127, 1271−1282.

5. *Methane coupling in nanosecond pulsed plasmas: Correlation between temperature and pressure and effects on product selectivity.* Eduardo Morais, Evangelos Delikonstantis, Marco Scapinello, Gregory Smith, Georgios D. Stefanidis, Annemie Bogaerts. 2023. Chemical Engineering Journal, Vol. 462, https://doi.org/10.1016/j.cej.2023.142227.

6. *Plasma-based dry reforming of CH4: Plasma effects vs. thermal conversion.* Joachim Slaets, Bj¨orn Loenders , Annemie Bogaerts. 2024. Fuel, Vol. 360, https://doi.org/10.1016/j.fuel.2023.130650.

7. *LXcat. Morgan database.* [Online] 2019. www.lxcat.net.

8. *Evaluated Kinetic Data for Combustion Modelling: Supplement II.* D. L. Baulch, C. T. Bowman, C. J. Cobos, R. A. Cox, Th. Just, J. A. Kerr, M. J. Pilling, D. Stocker, J. Troe, W. Tsang, R. W. Walker, J. Warnatz. *2005. J. Phys. Chem.*